# Measurement and Identification of the Nonlinear Dynamics of a Jointed Structure Using Full-Field Data; Part II - Nonlinear System Identification

Mengshi Jin[a,b], Giancarlo Kosova[c,d], Mattia Cenedese[e], Wei Chen[a,b], Aryan Singh[f], Debasish Jana[g], Matthew R. W. Brake[h], Christoph W. Schwingshackl[i], Satish Nagarajaiah[g,h], Keegan J. Moore[f], Jean-Philippe Noël[j]

[a]*AECC Shanghai Commercial Aircraft Engine Manufacturing Co. LTD., Shanghai, 201306, China*

[b]*School of Aerospace Engineering and Applied Mechanics, Tongji University, Shanghai, 200092, China*

[c]*Siemens Industry Software, Leuven, Belgium*

[d]*Aerospace and Mechanical Engineering Department, University of Liège, Liège, Belgium*

[e]*Institute for Mechanical Systems, ETH Zürich, Leonhardstrasse 21, 8092 Zürich, Switzerland*

[f]*Department of Mechanical and Materials Engineering, University of Nebraska-Lincoln, Lincoln, NE 68588, USA*

[g]*Civil and Environmental Engineering, Rice University, Houston, TX 77005, USA*

[h]*Department of Mechanical Engineering, Rice University, Houston, TX 77005, USA*

[i]*Imperial College London, Mechanical Engineering, Exhibition Road, SW7 2AZ London, UK*

[j]*Control Systems Technology Group, Department of Mechanical Engineering, Eindhoven University of Technology, NL*

---

## Abstract

The dynamic responses of assembled structures are greatly affected by the mechanical joints, which are often the cause of nonlinear behavior. To better understand and, in the future, tailor the nonlinearities, accurate methods are needed to characterize the dynamic properties of jointed structures. In this paper, the nonlinear characteristics of a jointed beam is studied with the help of multiple identification methods, including the Hilbert Transform method, Peak Finding and Fitting method, Dynamic Mode Decomposition method, State-Space Spectral Submanifold, and Wavelet-Bounded Empirical Mode Decomposition method. The nonlinearities are identified by the responses that are measured via accelerometers in a series of experiments that consist of hammer testing, shaker ringdown testing, and response/force-control stepped sine testing. In addition to accelerometers, two high-speed cameras are used to capture the motion of the whole structure during the shaker ringdown testing. Digital Image Correlation (DIC) is then adopted to obtain the displacement responses and used to determine the mode shapes of the jointed beam. The accuracy of the DIC data is validated by the comparison between the identification results of acceleration and displacement signals. As enabled by full-field data, the energy-dependent characteristics

of the structure are also presented. The setup of the different experiments is described in detail in Part I of this research. The focus of this paper is to compare nonlinear system identification methods applied to different measurement techniques and to exploit the use of high spatial resolution data.

*Keywords:* Jointed Structures, Nonlinear System Identification, Digital Image Correlation (DIC), Amplitude-Dependent Characteristics, Energy-Dependent Characteristics

---

## 1. Introduction

Mechanical joints are of crucial importance in the dynamics of assembled structures [1]. Significant nonlinearities can be caused by friction, wear, and non-idealized boundary conditions [2, 3, 4]. With slip and clapping behaviors happening between the interfaces [5], the complexity of the joints makes the modeling highly challenging. Therefore, it is extremely important to characterize the behaviors of jointed structures experimentally with high accuracy, which is a pressing need in several industries such as aerospace [6], automotive [7], and naval [8].

Among several tools available, backbone curves are a common method for describing nonlinear systems [9, 10] as they characterize the amplitude-dependent natural frequency and damping for single mode oscillations from free decay data [11]. The interactions that may occur in the system can be elucidated, enabling the investigation of modal energy exchange due to the nonlinearities, which cannot be analyzed by conventional linear system identification methods. Moreover, the backbone curve makes it possible to estimate or update the nonlinear characteristics within a model based on the experimental response [12, 13, 14, 15]. Even more so than frequency, damping is critical in predicting and understanding the behaviors of a structure [16, 17]. Often, the damping nonlinearity in a jointed structure changes the damping capacity of a structure by orders of magnitude across a range of response amplitudes while the stiffness nonlinearity changes the natural frequencies by a few percent [18]. The amplitude-damping curve is a general way to demonstrate the dissipation of systems [10], especially for jointed structures [1]. Together, the knowledge of amplitude-dependent damping and amplitude-dependent frequency characteristics can be used to make predictions for the steady-state forced harmonic response of a structure. The key to this is the single-nonlinear-mode theory, for which simple, explicit approximations are available [19, 20, 21].

There are many different methods for calculating the amplitude-dependent frequency and damping curves, hereafter also referred to as the frequency and damping backbone curves. The Hilbert Transform (HT) method [22, 23] is generally considered to be a reliable time-domain identification method [9] and relatively accurate compared with other identification methods [24]. The Peak Finding and Fitting (PFF) method [25] is another time-domain method, which is recently proposed based on the traditional zero-crossing (ZC) method [10]. One limitation of the above two methods is that they are mono-modal, i.e., they are formulated to analyze one mode and one point at a time and cannot identify modal interactions. One approach to address this shortcoming is the use of frequency-domain methods, such as the Dynamic Mode Decomposition (DMD) method, which finds coherent spatial-temporal pattern from the dataset [26]. When the dimension of acquisition is less than the rank of the system, the modified version of DMD, i.e., the Hankel DMD [27, 28], can be used to analyze the system. For analyzing vibrations of mildly nonlinear systems, the window based Hankel DMD can be used to obtain the time-varying modal parameters. A fundamentally different approach from time-domain and frequency-domain methods is the identification of the nonlinear normal modes of a system. Nonlinear normal modes (NNMs) [29] are a popular and useful tool for the analysis of vibrations in nonlinear, conservative systems. Similarly, Spectral Submanifolds (SSMs) [30] represent the extension of classical nonlinear normal modes to forced-damped nonlinear structures. SSMs can be exploited to gain precious insights on the dynamical behavior [31, 32] and to construct reduced-order models [33]. A methodology was proposed to analytically compute both the shape of SSMs and their corresponding backbone curves according to a data-assimilating model that was fitted on experimental vibration signals [34]. This means that a data-driven polynomial state space model can be constructed based on SSMs. Besides the aforementioned methods, time-frequency analysis is another powerful way to extract information about frequency and damping in structural dynamics. Empirical Mode Decomposition (EMD) is a technique that decomposes a signal into a finite set of intrinsic mode functions (IMFs) [35]. Wavelet-Bounded EMD (WBEMD) is an improvement over EMD, improving the separation of IMFs, which represent different characteristic time scales. In this manner, the WBEMD method is able to identify not just frequency and damping information, but also the portions of the time record that the information is extracted from, allowing an analyst to visualize how the system changes over time across a large range of frequencies [36]. These system identification methods are described more in detail in Sect. 2.

Nonlinearities are usually characterized by amplitude-dependent curves [9, 37], i.e., the frequency/damping is plotted as the function of the amplitude. The shortcoming of this representation is that the characterization of the nonlinearity is related to the amplitude of a certain accelerometer, thus a specific point/location. In the view of reaching a more global metric, attention has been paid to the relationship between the energy stored in a mode and the corresponding frequency characteristics (hereafter referred to as the frequency-energy relationship) [38]. While frequency-energy plots can be easily computed in analytical or numerical studies [29, 39], their experimental determination remains a challenge. The energy of a physical structure is difficult to calculate based on the information of either dense or sparse accelerometers.

With the development of high-speed cameras, the motion of the whole structure can be recorded by images with high spatial resolution. Digital Image Correlation (DIC) [40, 41] can then process the recorded images and extract displacements of the structure. Although they have lower accuracy, high-speed cameras perform non-contact measurements and allow higher spatial resolution than accelerometers. DIC has recently been applied to study jointed structures [5, 42] by measuring the slip and separation behaviors in the interfaces. Additionally, DIC has advantages over other non-contact measurement techniques, chiefly laser Doppler vibrometer (LDV). For instance, DIC is often a more affordable approach than LDV and the latter is also more time consuming, since a LDV has to scan across the surface one point at a time. The disadvantage of current DIC methods, though, is the large post-processing time to extract the large amount of data from videos of the experiment as well as limitations in memory for data storage.

The number of testing methods for extracting amplitude-dependent characteristics from nonlinear structures has been growing in the last two decades [38]. Hammer excitation or imposed initial conditions are used to trigger decaying oscillations [24], but they typically lack in isolating single mode responses. Another family of methods, such as force appropriation [43, 44] or control-based continuation [45], exploits mono-harmonic forcing from a shaker as well as the phase-quadrature criterion to isolate resonant vibrations and to extract amplitude-dependent properties. However, these methods can be excessively time-consuming and they can suffer from structure-shaker interactions. Resonance decay, or shaker ringdown testing [46, 47], has been introduced to solve these issues. Here, a high-amplitude resonant vibration is isolated via phase-quadrature using the shaker and, afterwards, the shaker is decoupled from the structure, which shows single-mode decaying responses. Although decoupling the shaker from the structure is not a trivial operation, the extraction of amplitude-dependent properties is faster with respect to other shaker-based methods.

This research consists of two parts. The first [48] focuses on experimental investigations, describing the tools, methods, and challenges for extracting the data from a benchmark system in vibrations of joint-assembled structures. Both accelerometers and high-speed cameras are adopted to record the motion of the system over time. In this work, the spatially dense data from [48] is analyzed in order to assess the efficacy of using DIC for nonlinear system identification. Multiple nonlinear system identification methods are utilized and compared with each other in order to establish their performances and to highlight pros and cons from a practitioner viewpoint. Both free decay vibration and forced-response testing are analyzed for the extraction of backbone and damping curves and, due to the availability of full-field data and energy estimations, their interconnections are investigated with novel metrics. Moreover, this research shows the agreement of data from the accelerometers and DIC and sheds further light on amplitude-dependent properties by inspecting the shape variations and the energy of the structure.

The paper is organized as follows. In Sect. 2, the different methods adopted are summarized. Section 3 reports on the analysis of experiments, first focusing on accelerometer data and then on DIC data, which comes from hammer testing, shaker ringdown testing, and response/force-control stepped sine testing. Additionally, an energy criterion is established to connect amplitude-dependent properties from forced-response testing with those obtained via free-decay response. Section 4 presents a critical comparison of the adopted methods, and Sect. 5 concludes the paper.

## 2. Nonlinear System Identification Methods

In this section, the five methods utilized throughout this research are briefly reviewed, including the Hilbert Transform (HT) method [22, 23], Peak Finding and Fitting (PFF) method [25], State-Space Spectral Submanifold (SS-SSM) method [34], Dynamic Mode Decomposition (DMD) method [27, 28], and Wavelet-Bounded Empirical Mode Decomposition (WBEMD) method [36]. Among these methods, the HT and PFF are time-domain approaches, the DMD belongs to frequency-domain method, the WBEMD is a time-frequency analysis method [9], and the SS-SSM is a data-driven modeling technique. Each of these methods are applied to analyze the data from different experiments in Sect. 3.

### *2.1. The Hilbert Transform Method*

Generally, the HT method is regarded as one of the most popular and reliable nonlinear system identification methods. It was proposed by Feldman [22, 23] and was applied to identify different nonlinear systems [49, 50, 51]. The sum of the signal and its HT composes the analytical signal. When the analytical signal is written in polar coordinates, the instantaneous amplitude and instantaneous frequency can be calculated. However, smoothing is needed for the identified characteristics [52]. There are a few ways to accomplish the smoothing, including filtering the identification results and mirroring the original signal before applying the HT method. According to [24], Empirical Modal Decomposition (EMD) [35] is an effective way that can be combined with the HT method to provide the smoothed results for both instantaneous amplitude and frequency. Based on the local time scale of the signal, EMD can be used to decompose the signal into intrinsic mode functions [35], the first of which generally contains the highest frequency components. By excluding the high frequency components, EMD is able to smooth the results identified by the HT method. This means that EMD serves as a lowpass filter, but, importantly, it does not introduce a phase shift [24]. After smoothing, the damping ratio can be calculated based on the two smoothed quantities.

### *2.2. The Peak Finding and Fitting Method*

The PFF method [25] is based on the zero-crossing (ZC) method [10], which calculates instantaneous frequency according to the time instants where the signal crosses zero. The identification accuracy of PFF was demonstrated by several cases in [24]. In the PFF method, the local maxima (and minima) of the signal are first searched. With the combination of the local maxima (and minima) and the two points near them, the signal near the local maxima (and minima) can be approximated by a polynomial. Therefore, improved estimations of the true values of the peaks (and valleys) are obtained from the fitted polynomial, which can overcome errors due to under-sampling. Then, the PFF method calculates instantaneous frequency as the reciprocal of the difference between two sequential time instants at which the signal reaches these peaks (and valleys). The PFF method is able to provide the result of the instantaneous frequency that achieves similar accuracy as the ZC method. Furthermore, by improving the extraction of the peaks, the instantaneous amplitude of the response can be obtained with higher accuracy by the PFF method. Therefore, the damping ratio, which is calculated by the instantaneous frequency and instantaneous amplitude, has less noise compared with that obtained by the ZC method [25]. Moreover, unlike the HT method, the instantaneous frequency and instantaneous amplitude calculated by the PFF method do not need to be smoothed, thus saving computational time.

### *2.3. The State-Space Spectral Submanifold Method*

A spectral submanifold (SSM) is referred to as the smoothest nonlinear continuation of a linearized mode shape of an equilibrium [30]. Thus, SSMs are calculated in order to analyze the reduced dynamics of the system, giving a nonlinear extension of the linear dynamics of the modal subspace. Moreover, the amplitude-dependent frequency curve along SSMs has been shown to approximate the backbone curve of forced frequency responses [11]. With respect to methods developed in the framework of conservative nonlinear normal modes [29], the theory of SSMs relaxes some critical assumptions on the purely parasitic effect of damping. Thus, the SS-SSM data-driven method developed in [34] puts no restriction on the type and magnitude of the damping; however, it does require that the signal being analyzed have a dynamic response that is sufficiently close to a single-mode (or two-dimensional) SSM of the underlying system. The data are simultaneously assimilated into a nonlinear discrete-time state space model from which the parametrization and the reduced SSM dynamics are analytically computed, giving a nonlinear extension of the linear dynamics of the modal subspace. The reduced-order model of the SSM is then exploited to derive amplitude-dependent properties. This approach was demonstrated to reproduce backbone curves with high accuracy according to the results of both numerical and experimental data [34, 53].

### *2.4. The Dynamic Mode Decomposition Method*

For the fluid dynamics community, DMD is one of the most promising system identification tools since it allows for high dimensional measurements. This algorithm finds coherent spatial-temporal patterns from a densely measured dataset [26]. In this paper, since dense spatial data is provided due to the combination of high-speed cameras and DIC, DMD is used to comprehend the underlying dynamics of the structure. As the rank of the structural vibration is much less than the dimension of data acquisition, this type of system identification technique is well suited. Also, for the cases when only one accelerometer is used, this technique is still able to provide accurate information about the modal parameters of the system. In the present context, the modified version of DMD, known as Hankel DMD [27, 28], is used to analyze the system. The formulation of Hankel DMD is similar to the formulation of the Eigensystem Realization Algorithm [28, 54] that is typically used for system identification of linear dynamical systems. Hence, in this study, for analyzing the vibration of the jointed structure that is a mildly nonlinear system, window-based Hankel DMD is used to capture the time-varying modal parameters of the structure. It is assumed that in a small time window, this mildly nonlinear structure approximately behaves like a linear dynamical system. Amplitude information is obtained via filtering at frequencies of interest.

### 2.5. The Wavelet-Bounded Empirical Mode Decomposition Method

By exploiting EMD, a signal is decomposed into a finite set of nearly orthogonal, monochromatic intrinsic mode functions (IMFs) [35, 55]. Theoretically, every IMF should be a physical and mathematical representation of a single characteristic time scale contained in the original oscillatory signal. However, in practice, EMD yields spurious, non-physical IMFs, which need to be eliminated before starting the dynamical analysis [56]. Another issue with the regular EMD is the problem of mode mixing, where one IMF is comprised of components at different frequencies and, thus, is not a fair representation of any single time scale extracted from the original signal. The WBEMD augments the regular EMD by using a masking signal, which provides a quantitative measure of the isolation of an IMF around a characteristic frequency [36]. This measure is used as the objective function of a minimization problem. In the WBEMD algorithm, after applying EMD, the IMF is transformed into the maximum wavelet domain [57] where a bounding function is fitted over the IMF. This procedure is able to extract optimally-separated IMFs, each representing distinct time scales present in the signal. Once frequency information is obtained, ad-hoc filtering is applied to retrieve amplitude and damping characteristics of the signal.

## 3. Analysis of Experiments

Using the nonlinear system identification methods described in the previous section, the experiments on the Half Brake-Reuß Beam (HBRB) described in [48] are analyzed. These experiments include hammer testing, shaker ringdown testing, and response/force-control stepped sine testing. **Figure 1** summarizes the experiments, along with the pre-processing techniques and the identification method used to extract nonlinear information. The HBRB is modified from a normal BRB [1], which is a prismatic 304 stainless steel beam joined in the middle through a three-bolt lap joint (**Fig. 2**), to be half of the nominal thickness. This modification was chosen in order to reduce the first three natural frequencies of the system such that high-speed videography could easily measure the response of the first three modes without sacrificing spatial resolution. The nonlinear characteristics extracted from the hammer testing and shaker ringdown testing are compared with the backbone curves extracted directly from the response/force-control stepped sine testing [48].

During the shaker ringdown testing, apart from accelerometers, two high-speed cameras are used to capture images of the HBRB. DIC [40, 41] is applied to the images, providing the displacement responses of the beam. The specific set of measurements used from each experiment are further highlighted in the flowchart of **Fig. 1**. During this study, each bolt is tightened to 10 N·m and the first mode is mainly considered (except where noted otherwise). Further details of all of the experiments in this section can be found in Part I of this research [48].

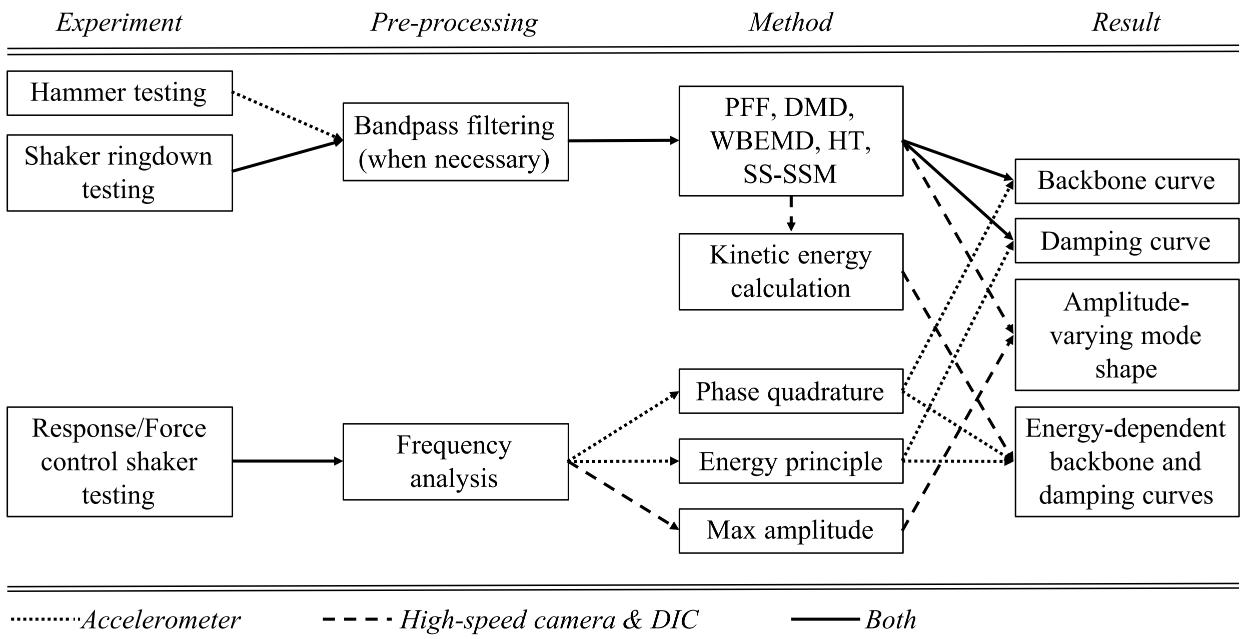


Figure 1: Flowchart that represents the experiments and the methods discussed in this paper, also including the necessary pre-processing and the identification results. Different measurements, from accelerometer or speed camera, are highlighted using different linestyles.

### *3.1. Free Decay Response by Accelerometers*

In this section, the identification results from free decay responses of accelerometer measurements are discussed. Specifically, the amplitude-dependent properties extracted via hammer testing and shaker ringdown using the methods presented in Sect. 2 are discussed.

#### *3.1.1. Hammer Testing*

During the hammer testing of the HBRB, free boundary conditions are achieved by hanging the beam with the combination of fishing lines and bungees [48, 15]. The constraints (at the node points of the first mode) are applied since the beam should be confined within a limited space, and it is demonstrated in Part I that the specific arraingements of constraints used here do not significantly affect the characteristics of the beam [48]. The HBRB is excited by the hammer and is measured by three accelerometers (**Fig. 2**) with a sampling frequency of 6400 Hz. As an example, a free decay response obtained by the accelerometer nearest to the impact location (indicated as Accel 3 in **Fig. 2**) is shown in **Fig. 3** (a).

With the time history response, the methods described in **Sect. 2** are applied to obtain backbone curves and amplitude-damping curves of the HBRB, with the exception of the SS-SSM method. This method is excluded since it assumes that the data are dominated by a single-mode SSM, which is not the case in hammer testing.

The backbone curves extracted in this section are defined as the amplitude-frequency relations of principal modes, or components, of the decaying signals. Since the HT and

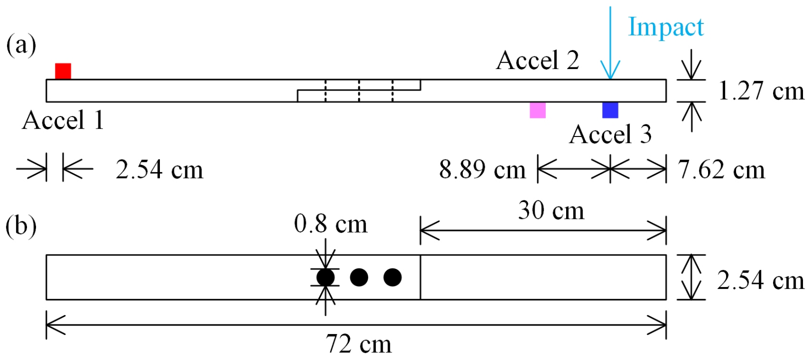


Figure 2: The setup of the hammer testing for the HBRB, showing from the (a) top and (b) side views.

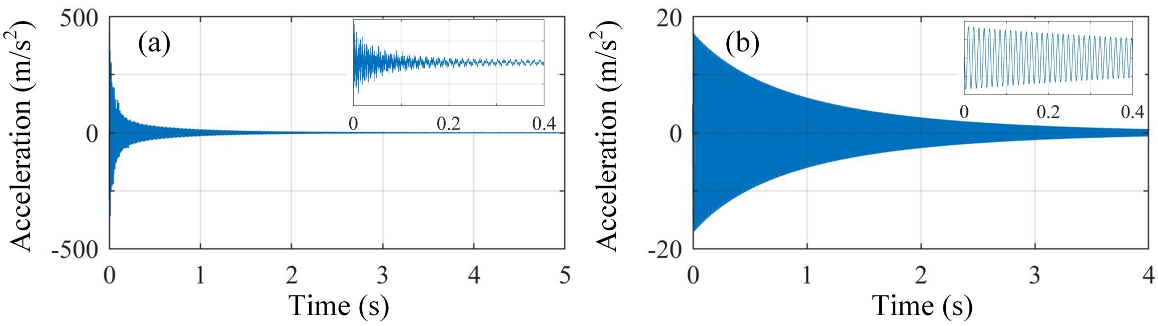


Figure 3: The free decay response measured by Accel 3, showing (a) raw response (with zoomed response from 0 s to 0.4 s) and (b) filtered response (with zoomed response from 0 s to 0.4 s).

PFF methods can only be applied to a signal with one frequency component, the free decay response has to be filtered [58] before these two methods are applied. The effects of applying a third-order butterworth bandpass filter whose frequency band is from 75.27 Hz to 85.27 Hz are shown in **Fig. 3 (b)**. The acceleration response is truncated at 4 s to obtain the identification results with a high signal-to-noise ratio. Additionally, for the HT method, the signal is further truncated from 0.5 s to 3.9 s so that the end effects can be reduced.

As shown in **Fig. 4**, all of the different methods show great agreement in the identification of both the backbone curve and amplitude-damping curve for the first mode. This means that the instantaneous frequency, amplitude, and damping ratio are well identified by these methods. The change in damping (from 0.13% to 0.25%) as the response amplitude increases from 0.4 m/s$^2$ to 17 m/s$^2$ is significantly greater than the change in frequency (from 80.3 Hz to 80 Hz), which is typical in the context of jointed structures.

The spikes observed in the damping curve obtained by the HT method are caused by the calculation of the damping ratio, which is related not only to the amplitude, but also to its derivative [25]. Thus, although the signal was already truncated before using the HT method, there are still errors at the two ends in the damping ratio, which is one of the drawbacks of the HT method.

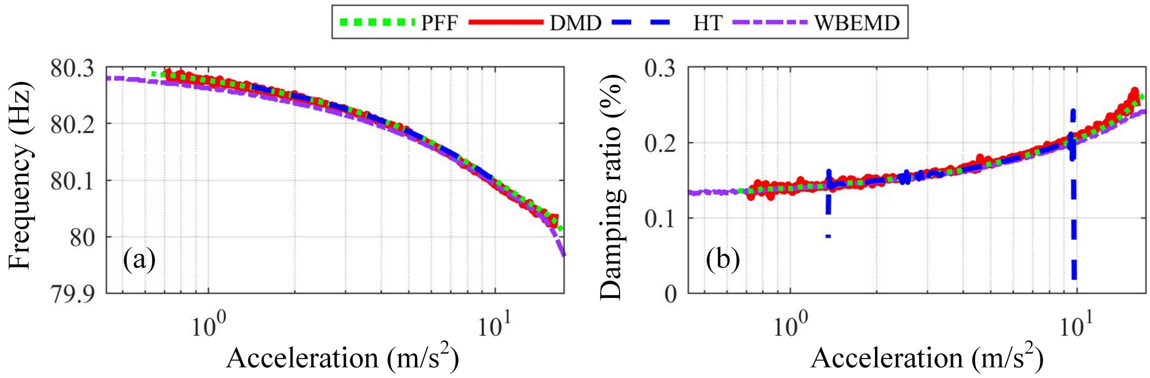


Figure 4: The identification results of the hammer testing by the PFF (green dotted line), HT (blue dashed line), DMD (red solid line), and WBEMD (purple dash-dotted line) methods, showing (a) backbone curve and (b) amplitude-damping curve.

In comparing the PFF, DMD, and WBEMD methods, the PFF and DMD method both overlay the HT method, while the WBEMD method results in slightly lower predictions, both for frequency and damping. This is justified by the fact that WBEMD does not pre-filter the signals, in contrast with the other methods. Lastly, both the PFF and WBEMD show significantly less noise, especially in measurements of damping, than the DMD and HT methods.

### *3.1.2. Shaker Ringdown Testing*

With the experimental setup similar to that of the hammer testing, shaker ringdown testing for the first mode of the HBRB is performed. The shaker is attached to the same location as the hammer impact point in **Fig. 2** and it is used to obtain approximately single-mode responses [59]. After isolating a resonant frequency response (reaching a 90-degree phase lag between force and driven point) or NNM, the shaker is physically detached from the HBRB [60], and the system decays to the equilibrium along the related SSM [30], as illustrated in **Fig. 5**. See [48] for a more detailed description of the experiment. Hence, the backbone curve computed is the SSM free decay instantaneous frequency-amplitude relation. Apart from the three accelerometers, two high-speed cameras are used to measure the displacement of the beam. DIC [40, 41] is applied to the captured images to acquire the displacement responses. The analysis of the displacement responses is presented in Sect. 3.3, while this section focuses on the acceleration measured by the accelerometer located on the shaker excitation point.

The Short-time Fourier transform (STFT) analysis is conducted on the response of the shaker ringdown testing. As it can be seen from **Fig. 5** (b), the energy is only in the first mode (below 100 Hz) and it stays in the first mode, except at the moment when the shaker is decoupled from the beam; however, the effect shown by the STFT analysis (Fig. 5(b)), does not persist past 30.2 seconds, which is where the signal is truncated for analysis. All of the methods described in **Sect. 2** are applied to the signal from time 30.2 s

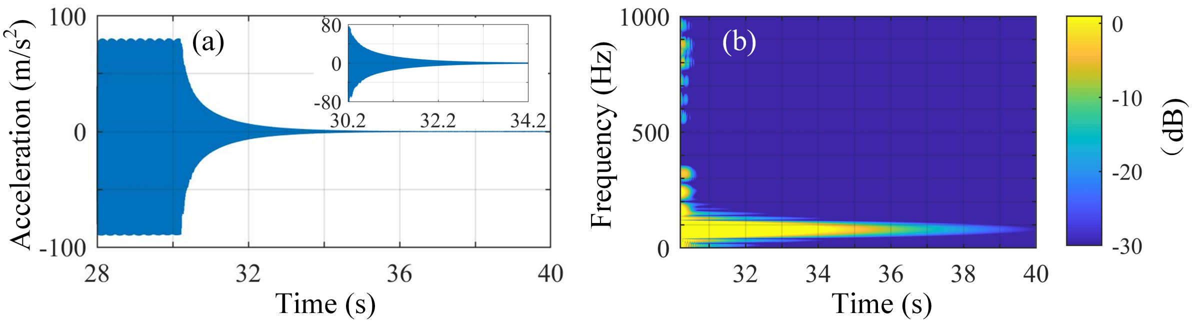


Figure 5: The acceleration response measured by Accel 3, showing (a) raw response from 28 s to 40 s (with zoomed response from 30.2 s to 34.2 s) and (b) STFT analysis of the response from 30.2 s to 34.2 s.

to 40 s (i.e., from the moment that the shaker is decoupled from the system until the noise floor is reached). It is shown in **Fig. 6** that there is little difference in the identification results, which means that the instantaneous frequency, amplitude, and damping ratio are all identified with similar accuracy by these methods, with several exceptions discussed in what follows. The instantaneous damping ratio rises with the amplitude increasing, from about 0.1% to more than 0.6% (**Fig. 6** (b)). Thus, a strong nonlinearity in the damping of the HBRB is observed. The instantaneous frequency undergoes small variations (0.5 Hz, or 0.6%) in this amplitude regime. Unlike the impact hammer tests, which were limited in terms of the amount of energy that they could put into a single mode and could not drive the system to a high enough amplitude to make this observation, the shaker ringdown experiments exhibit a softening-hardening trend as the amplitude increases (**Fig. 6** (a)). As shown in the next sections, this trend is not a characteristic of this specific accelerometer, but rather of the whole structure.

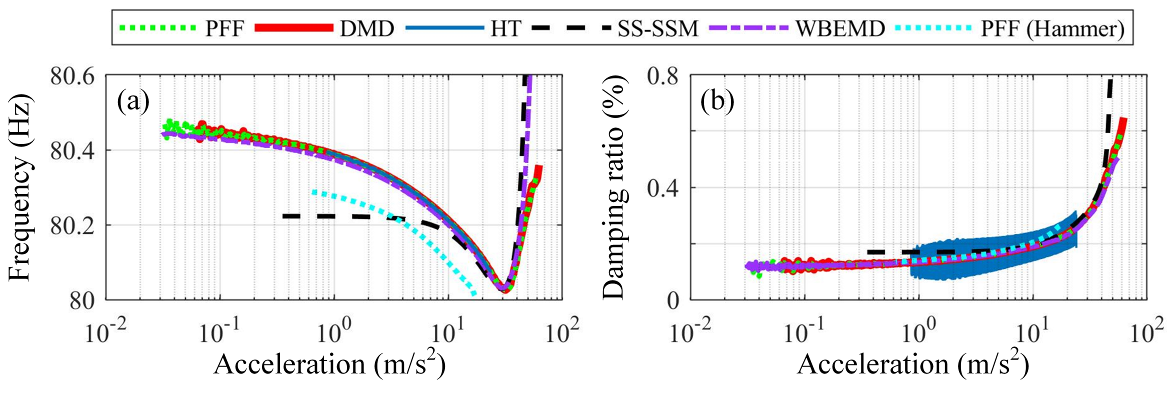


Figure 6: The identification results of the shaker ringdown testing by the PFF (green dotted line), DMD (red thick line), HT (blue thin line), WBEMD (purple dash-dotted line), and SS-SSM (black dashed line) methods, showing (a) backbone curve and (b) amplitude-damping curve. The cyan dotted lines are the identification results of the hammer testing using the PFF method.

One challenge for analysis is that most methods (e.g., the PFF method) are only capable of dealing with a signal that contains exactly one frequency component. Thus, although the free decay response of the shaker ringdown testing can be approximately regarded as the signal with single frequency, the response is still filtered by the third-order butterworth bandpass filter (that is used in the hammer testing) before the PFF method is applied. The identification results of the HT method have much fewer data points than the other methods, since the curves have been truncated to avoid the end effects [52]. Although the identified frequency is smoothed [35] before being used to calculate the damping ratio, the corresponding damping ratio shows the most noise among all of the methods. The results obtained by the WBEMD method slightly differ from those of the others at high amplitudes.

The SS-SSM method, with respect to the other signal processing ones, analyzes the dynamics of a discrete-time state space model fit on the signals shown in **Fig. 5** (a). The results in **Fig. 6** have been obtained using a 6-dimensional system with polynomial nonlinearities up to order 5. The state space is made of measurement delays (using the typical settings of autoregressive-moving-average models [34]), and the SSM expansion is then carried out up to order 19. There is a discrepancy in the frequency of the SSM model and those of the other backbones for low amplitudes since the SSM model has a well-defined linearized frequency that, along with the model nonlinearities, is optimized in order to minimize the model prediction errors.

Although **Fig. 4** and **Fig. 6** both show the results from free decay responses, these two tests have their own characteristics. To further compare the results from the two tests, the backbone and amplitude-damping curves obtained by the PFF method are presented in **Fig. 6**. This figure shows that the highest amplitude in the identification results of the shaker ringdown testing (80 m/s$^2$) is significantly larger than that of the hammer testing (20 m/s$^2$). This shows that the shaker ringdown tests are able to acquire a wider range of amplitudes than the hammer testing, providing more information about the variation of the amplitude-dependent frequency and damping ratio. This is due to the broadband nature of the hammer excitation in contrast with the possibility to isolate a single mode without appreciably exciting the other modes with shaker ringdown testing. Specifically, the initial acceleration in the hammer testing reaches 500 m/s$^2$ (**Fig. 3** (a)), while the acceleration of the shaker ringdown testing approaches only 100 m/s$^2$ (**Fig. 5** (a)). However, the response containing only the first mode has the initial acceleration of 20 m/s$^2$ in the hammer testing (**Fig. 3** (c)), and 80 m/s$^2$ in the shaker ringdown testing (the zoom in **Fig. 5** (a)). Thus, most of the energy is dissipated along a single mode or SSM in shaker ringdown testing, while hammer testing allows the interplay of multi-modal nonlinear dissipation. As evidenced in **Fig. 6** by the discrepancies between the amplitude properties, other frequency components present in the signal influence the amplitude curves of the first mode, even though proper filtering is performed. Therefore, if the aim of testing is to study modes in isolation, shaker ringdown testing should be preferred due its capability to isolate single modes and to obtain larger amplitude ranges.

### *3.2. Forced-response Testing*

The forced-response testing aims at validating the previous free decay results. The instantaneous frequency-amplitude curve of decaying vibrations has been often observed to serve as a backbone for the frequency response for small forcing [46, 47, 43, 61, 62] (in particular in [63, 64, 21] for non-conservative systems), and this relation is formally established in [11]. Specifically, the backbone curve of a single mode SSM is the leading order approximation of frequencies and amplitudes at which forced response maxima occur for different forcing values.

In this research, both response-amplitude-control and force-amplitude-control stepped sine testing are conducted on the HBRB for extracting forced responses. These are measured by accelerometers to identify the backbone and amplitude-damping curves. The difference between the two types of testing is that, in the response-amplitude-control testing, the response amplitude of the driven point is controlled to be constant. By contrast, the amplitude of the shaker force is controlled to remain fixed in the force-amplitude-control testing. Since the first mode of the HBRB is concerned, the excitation frequency is swept from 79 Hz to 81 Hz with the step of 0.05 Hz. The response-amplitude-control testing is conducted with amplitudes of 0.5 g, 2 g, 4 g, 5 g, 6 g, 7 g, and 8 g, and the force-amplitude-control testing contains the force levels of 0.2 N, 0.5 N, 1.0 N, and 1.5 N. More detailed description of the forced-response testing can be found in Part I [48]. **Figure 7** (a) shows the measured response amplitude for the two types of forced testing, depicting the response-control testing in red and in green the force-control testing. In what follows, the principal harmonics in force and acceleration signals are only considered as higher order harmonics have negligible influence for the system under analysis, cf. **Sect. 3.4.1**.

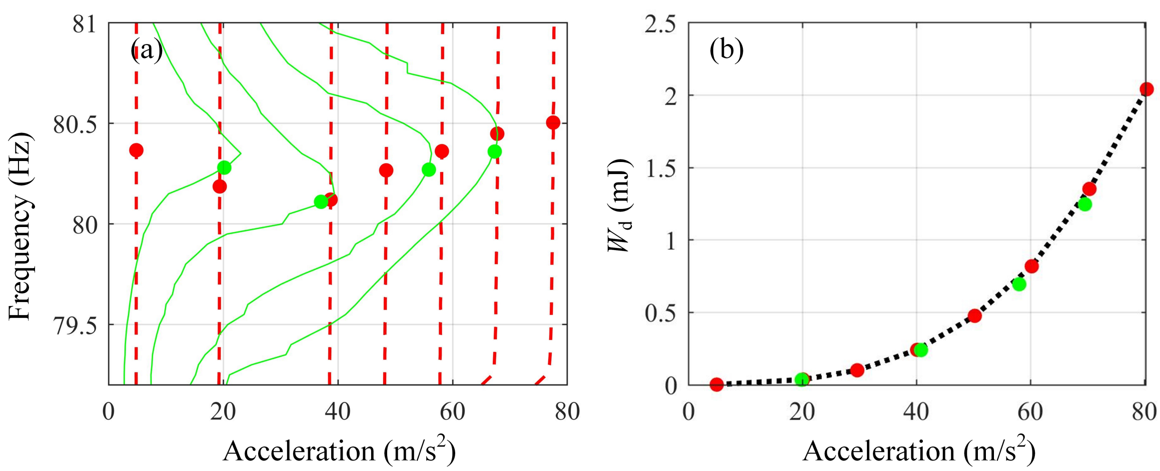


Figure 7: The results of the forced-response testing, showing (a) measured response amplitude in the response-control testing (red dashed line) and force-control testing (green dashed line) with the respective resonance frequency indicated with circles, and (b) dissipated energy over one oscillation cycle at resonance frequencies shown with consistent colors. Here, the black line connects red markers.

The extraction of maximal or resonant responses is performed by selecting the responses satisfying the quadrature phase-lag criterion [46, 44, 61]. Here, the displacement response of the driven point has approximately a 90° phase lag with respect to the forcing signal. The identification of the backbone curve is then straightforward for both tests and is indicated by circles in **Fig. 7** (a). The identification of the damping ratio, however, is not as immediate. For a periodic trajectory of a mechanical system, the energy principle states that the work done by non-conservative forces must be zero in one oscillation cycle [63, 44]. In other words, the input energy provided by the shaker $W_{\mathrm{a}}$ is dissipated, mainly due to friction occurring at the interface. **Figure 7** (b) shows the energy dissipated $W_{\mathrm{d}}$ in one cycle of resonant oscillation. By denoting the first harmonic component of the acceleration of the driven point response $\ddot{q}(t) = -A\sin(\Omega t)$, the forcing amplitude $F$, and the resonant forcing frequency $\Omega$, it holds that

$$W_{\mathrm{a}} = \int_0^{2\pi/\Omega} \dot{q}(t) F \cos(\Omega t) dt = \frac{\pi A F}{\Omega^2}, \tag{1}$$

and the dissipated energy over one oscillation cycle is

$$W_{\mathrm{d}} = \int_0^{2\pi/\Omega} 2m^* \zeta_A^* \Omega \dot{q}^2(t) dt = 2m^* \zeta_A^* \frac{\pi A^2}{\Omega^2}, \tag{2}$$

where $m^*$ is the equivalent modal mass. An equivalent, amplitude-dependent, modal damping ratio $\zeta_A^*$ can be determined from the equality $W_{\mathrm{a}} = W_{\mathrm{d}}$

$$\zeta_A^* = \frac{F}{2m^* A}. \tag{3}$$

The modal mass is estimated by calibration with the results from the free decay response, which results in $m^*$ =1.55 kg. Another computation of the dissipated energy is introduced later in **Sect. 3.4.3** exploiting full-field data from DIC.

The comparison between amplitude properties extracted from forced testing and the ones from free decay response are shown in **Fig. 8**. The results of the response-control and force-control testing are close to each other. Additionally, the results of the two forced-response testing are in good accordance with those of the shaker ringdown testing, especially in the curves of damping. Although there is some discrepancy in the identification of frequency, the trend of the backbones obtained by the forced-response testing is the same as that obtained by the shaker ringdown testing. The partial discrepancy could be justified by the low resolution (0.05 Hz) of forced testing, some control limitations at low amplitudes, and the influence of the metallic stinger used to attach the beam to the shaker. The latter results in an overall stiffness increase, consequently shifting the frequencies as shown in **Fig. 8** (a). Moreover, from Eqs. 1-3, the ratio between the external forcing amplitudes $F$ and those of the inertial forces $m^*A$ is equal to $2\zeta_A^*$, which stays small, thereby justifying the comparison between the results obtained via free decay response and forced response.

Although the response-control and force-control stepped sine testing are both capable of identifying nonlinear characteristics with high accuracy, they have several drawbacks. First, the identification is generally sparse as forced experiments require a considerable amount of time. Additionally, at least for the system under investigation, the experimental equipment showed limitations in reaching low amplitude levels of excitation.

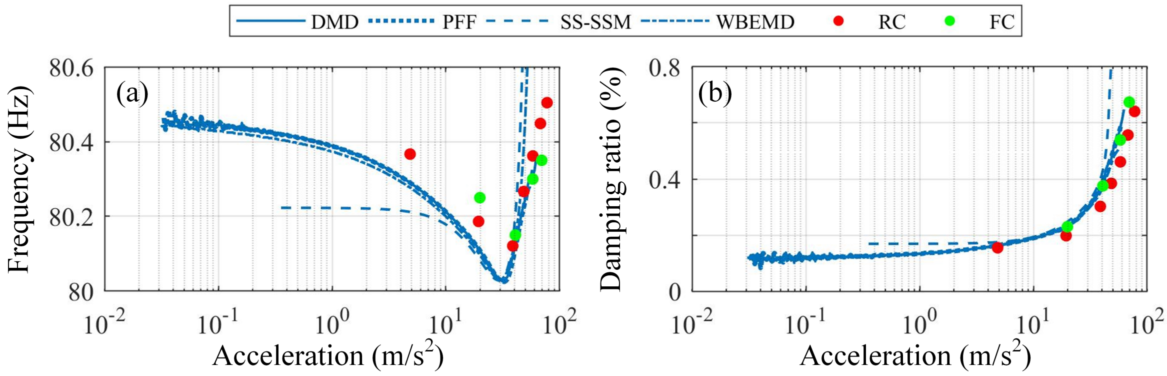


Figure 8: The identification results of the response-control testing (red circles), force-control testing (green circles), and shaker ringdown testing (blue lines) using different identification methods, showing (a) backbone curve and (b) amplitude-damping curve.

### *3.3. Free Decay Response by DIC*

Following the analysis of the accelerometer data in the previous section, this section focuses on the measurements from the two high-speed cameras, which are used to capture the displacement of the HBRB during the shaker ringdown testing. DIC [40, 41] is applied to the recorded images to calculate the displacement responses. Since there are multiple points in the images, the raw response and the filtered response (filtered by the same butterworth filter that is used in the hammer testing) of one of the points are selected to be shown in **Fig. 9**. The raw response mainly contains the first mode of the HBRB. Although the decaying signals shown in **Fig. 5** (a) and **Fig. 9** (a) comes from the same experiment, the presence of other frequency components is more evident in **Fig. 9**. In particular, the oscillation due to sway mode of the beam, at low frequency, is clearly visible, especially at the initial time instances of the measurement. The reason why it is more visible in the DIC data of **Fig. 9** (a) than in the accelerations in **Fig. 5** (a) is that DIC processes displacements, which are more evident at low frequencies.

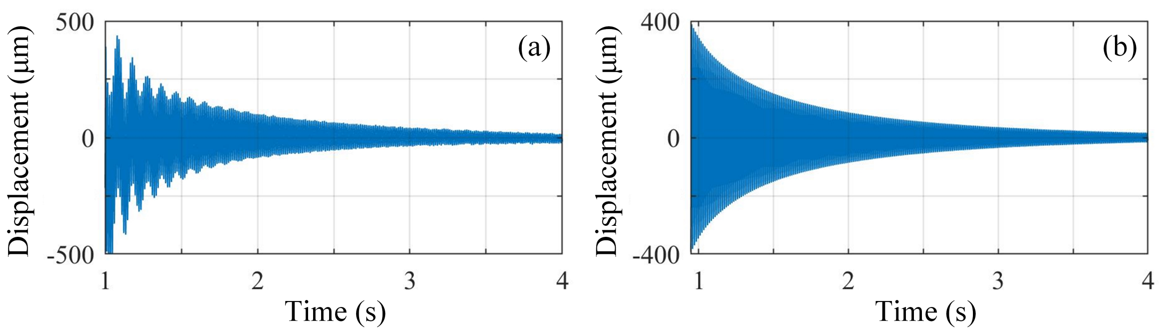


Figure 9: The displacement response of one of the points of the HBRB in the shaker ringdown testing, showing (a) raw response obtained by DIC and (b) filtered response.

Since all of the methods have already been compared when dealing with the acceleration signal in the hammer testing and shaker ringdown testing in **Sect. 3.1**, only the PFF and DMD methods are applied here to the displacement responses obtained via DIC. An important distinction between the two methods is that the PFF method is applicable to the response signal of one single point, while the DMD method is based on the Hankel matrix and can thus be applied to the response signals of all of the points together. In other words, given a large number of displacement responses, the PFF method will provide multiple curves, each of which corresponds to one of the points, and the DMD method will result in only one curve that contains the information of all of the points.

Note that the time series obtained from DIC have different signal-to-noise ratios across the length of the beam. In particular, time series whose locations lie close to the nodes of the mode shape are predominantly affected by noise. Additionally, during a free decay, signal-to-noise ratios worsen as time increases so that the time series have to be truncated to preserve a high signal-to-noise ratio.

The traditional way to present the backbone curve of a structure is to plot the frequency as a function of the response amplitude. **Figure 10** shows the identification results of the PFF method regarding the backbone curves and amplitude-damping curves of the measurement points on the beam.

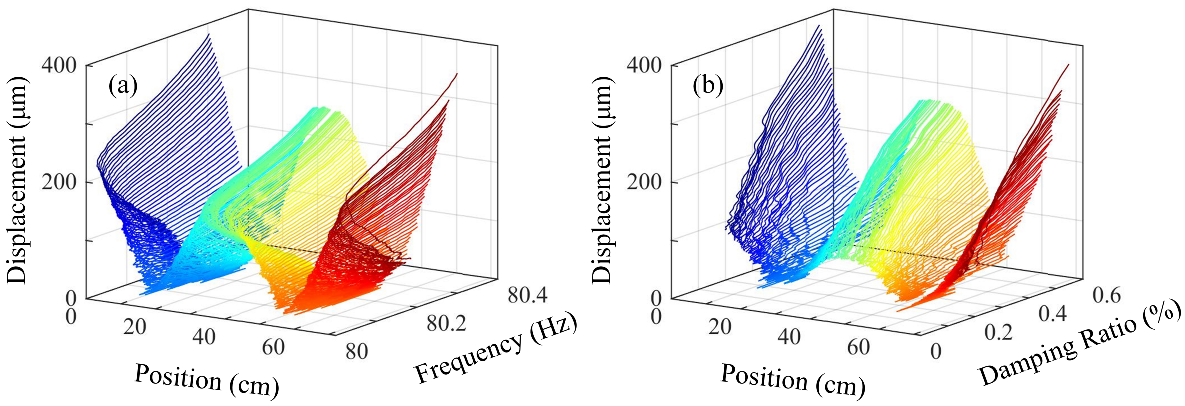


Figure 10: The identification results of the DIC data using the PFF method, which correspond to the measurement points at different positions, showing (a) backbone curves and (b) amplitude-damping curves.

It can be seen from **Fig. 10** that although the range of the frequency/damping ratio is the same for each point, the range of the displacement amplitude differs. Since all of the points are in different positions on the beam, the amplitude of each point is different from each other. Thus, it may not be particularly meaningful to express the frequency or damping ratio as a function of the displacement amplitude. Another way to normalize the response is to plot the frequency and damping ratios as a function of time, i.e., the instantaneous frequency and instantaneous damping ratio. The results of both the PFF and DMD methods are shown in **Fig. 11**, whose x-axes appear reversed when compared to amplitude-based plots, cf. **Fig. 6**.

Regarding the displacement responses obtained by DIC, both the PFF method and the

DMD method bring about similar results of the instantaneous frequency and damping ratio. As the PFF method is applied to the response signal of each measurement point, it provides a large number of curves whose variability is recast to noise effects. By contrast, because the DMD method combines the response signals of all of the points together and calculates one curve for each amplitude-dependent characteristic, the results of the DMD method can be regarded as the average of those obtained by the PFF method. Moreover, the instanteneous frequency and damping ratios from DIC data are consistent with those from accelerometer, as show in **Fig. 11** which includes the curves obtained via DMD from accelerometer data. However, acceleration signals have longer time histories than those obtained by the DIC data due the memory of the cameras. In particular, videography-based techniques are limited by the trade-off between spatial resolution and sampling frequency, which both determine the maximum length of the time signals possible based on available camera memory.

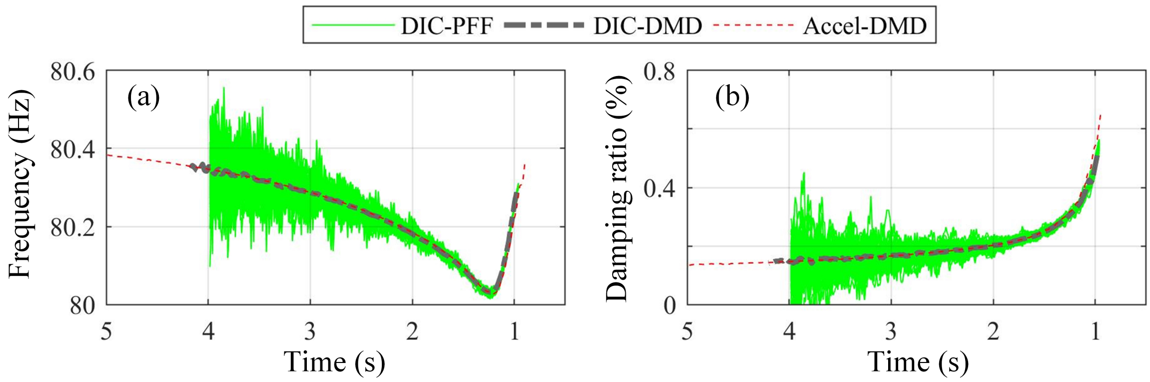


Figure 11: The results obtained by the DIC data and acceleration data using PFF (green solid lines) and DMD (grey dashed-dotted line for DIC data and red dashed line for acceleration data) methods, showing (a) instantaneous frequency and (b) instantaneous damping ratio.

### *3.4. Additional Information Brought by DIC*

Unlike the accelerometers that are sparsely distributed on the beam, the cameras are able to measure the displacement of an entire face of the HBRB, so that all of the points on the beam are recorded simultaneously. After the images are processed by DIC, the full-field information of the beam is available (i.e., the displacement responses of the points are obtained). Hence, DIC data allows the detailed analysis of the beam's mode shape and also the evaluation of its energy. Note that a similar degree of information cannot be achieved by accelerometers since it is difficult to place dense accelerometers on the structure without changing its characteristics at the same time [15].

#### *3.4.1. Measurements of Mode Shapes from Ringdown Testing*

In shaker ringdown testing, the motion of the beam during the free decay can be assumed as an estimation of the mode shape of the considered mode, since the beam is released from the quadrature between force and acceleration of the driven point [48]. The dominance of the fundamental harmonic during the decay is shown in **Fig. 5** (b) and the motion synchronism is further discussed and verified both at the end of this subsection and in **Fig. 13**. The mode shape is calculated as the deflection of the beam at each maximum of the cycle of motion. In this way, the time-varying (and thus, amplitude-varying) mode shape is obtained. The number of measurement points depends on the spatial resolution chosen for DIC [40, 41] [48]. The ultimate result consists of two lines describing the mode shape of the upper and lower part of the beam. These lines are displayed on a sketch of the beam in **Fig. 12** (a).

In **Fig. 12**, the shape of the first mode over 3.5 s of free decay is shown. This time duration is approximately 277 cycles of vibration; for visualization purposes, only 30 time instants are presented in **Fig. 12**. The abscissa is the position of the measurement points and the ordinate (Y axis) shows the amplitude of the responses of the corresponding measurement points. Each line consists of 206 DIC data points. It can be seen from **Fig. 12** that the amplitudes of the mode shapes reach zero at around 17 cm and 55 cm, which are the two positions of the node points of the first mode. Additionally, there is a discontinuity of the curvature of the mode shape at 29.7 cm for the lower line (blue) and at 42.3 cm for the upper line (red). These locations correspond to the left and right edges of the interface between the two half beams, shown in **Fig. 12** (a). When the amplitude of motion increases, the described discontinuity intensifies, due to the geometry of the beam. The mode shapes in **Fig. 12** refer only to the maxima of the cycle of motion, i.e., a deflection downwards of the center of the beam and upwards of the extremities. By contrast, the nodes of the mode shape preserve their location when motion amplitude changes.

The discontinuity in the mode shape is due to the opening of the interface on the lower edge (**Fig. 12** (c)), and closing of the interface on the upper edge (**Fig. 12** (d)). This behavior is also visible in **Fig. 12** (b), which reconstructs the maximum modal displacement of the entire beam from the two lines of that come from the DIC processing (**Fig. 12** (a)), and is consistent with other measurements of a similar lap joint [65, 66]. The difference between the upper and lower lines shows that the maximum and minimum differences occur at the locations of the discontinuities (29.7 cm and 42.3 cm (**Fig. 12** (e)), clearly reflecting the gap opening at the interface. However, the deflection ratio between upper and lower lines, depicted in **Fig. 12** (f), does not reveal significant variations over time.

Full-field data can also be used to assess whether the decaying vibrations shows synchronism or not. According to the original definition of a conservative nonlinear normal mode by Rosenberg [67], a periodic motion is synchronous if all maxima and minima of the position time series are achieved at the same time. Due to the presence of damping, synchronous motion is not guaranteed, but resonant motions in weakly damped structures have been still observed to be (approximately at least) synchronous [46, 47]. In **Fig. 13** (a), a time-extract of the full displacement field for the lower line of the beam is illustrated, where the abscissa displays time, cf. **Fig. 7** (b), the ordinate displays the position along the beam, and the color scale depicts the displacement magnitude. The horizontal white lines that appear from the colormap correspond to the nodes of the mode shape, while the vertical white lines show the times at which all of the responses are equal to zero. At least for this time portion, the decaying motion may already appear synchronous. This fact has also been verified in detail

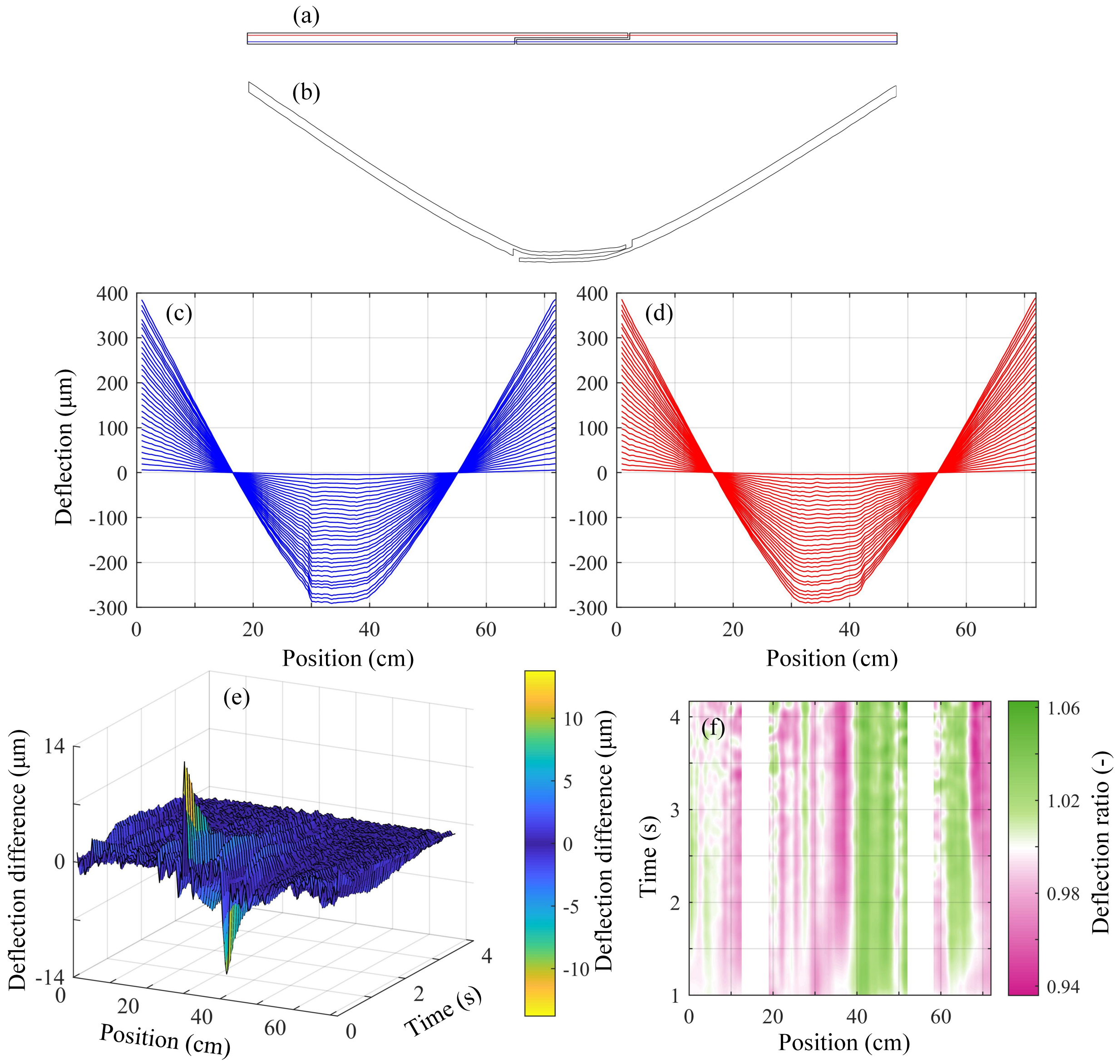


Figure 12: Amplitude-dependent mode shape of the $1^{st}$ mode of the HBRB from shaker ringdown testing, showing (a) sketch of the HBRB with the two lines identified with DIC, (b) maximum deflection shape, (c) DIC lower line, (d) DIC upper line, (e) difference, and (f) ratio between upper and lower line.

exploiting the PFF method, which computes the time at which a local extremum (either maximum or minimum) occurs for every displacement time series. Let $t_{ext}(l,k)$ be the time at which the $k$-th extremum occurs at the location $l$ and, by calling $\Omega$ the location domain, a metric to describe the synchronous behavior of the system is defined as

$$\Delta S(k) = \max_{l\in\Omega} |t_{ext}(l,k) - \bar{t}_{ext}(k)|, \qquad \bar{t}_{ext}(k) = \frac{1}{|\Omega|}\sum_{l\in\Omega} t_{ext}(l,k). \tag{4}$$

The quantity $\Delta S(k)$ acts as a metric for assessing the degree of synchronism in the structure and it is plotted in **Fig. 13** (b) once normalized by the sampling time $t_{samp} = 0.0002$ s. For computing $\Delta S(k)$, the points close to mode shape nodes have been excluded from the calculation domain $\Omega$ since their displacement time series are dominated by noise. Moreover, the increasing variability of $\Delta S$ over time is due to the deterioration of the signal-to-noise ratio for decreasing motion amplitudes. This analysis leads to the conclusion that the time at which an extremum is detected for a particular location differs by less than one sampling interval from the average time at which the same extremum is detected at any other location across the beam. A similar result holds for the times at which the displacement field is zero. Hence, the decaying vibration can be approximated as synchronous and this evaluation has crucial consequences for the evaluation of the energy and the mode shape of the beam, as discussed in **Sect. 3.4.3**.

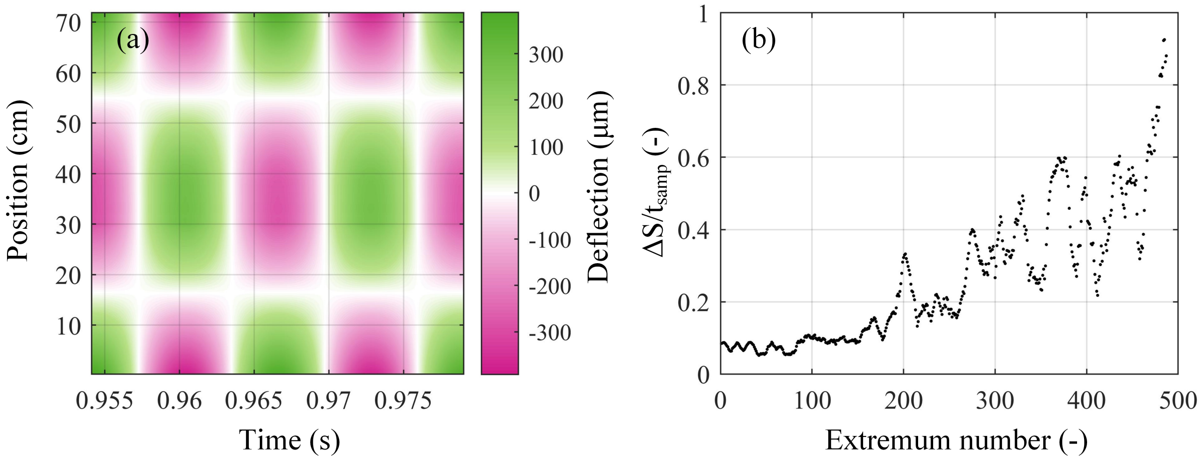


Figure 13: Assessment of motion synchronism, showing (a) full-field motion of the beam lower line for a selected time interval and (b) variability of the peak time identified via the PFF method.

### *3.4.2. Measurements of Mode Shapes from Response-Amplitude-Controlled Fixed Sine Testing*

Further information of the beam's mode shape can be extracted from response-amplitude-controlled fixed sine testing. The mode shape can be estimated from the time series, which has a controlled frequency, unlike the decaying vibrations measured in the ringdown tests. As the fixed sine testing is conducted to ensure that the system achieves a steady state response, multiple forcing cycles of the steady state response are able to be measured for each excitation amplitude. Tests are conducted for the response levels 0.5 g, 2 g, 4 g, 8 g, and 10 g, and the shaker is tuned for each amplitude to excite the first mode, as described in [48]. The same considerations of **Sect. 3.4.1** about the synchronism of the motion apply here. Moreover, **Fig. 14** shows the response spectrum of the beam extremity for the highest level of the excitation, where the higher harmonics are larger. The peaks below 8 Hz are rigid body modes, and the peak at 146 Hz is due to the fan internal to each of the high-speed

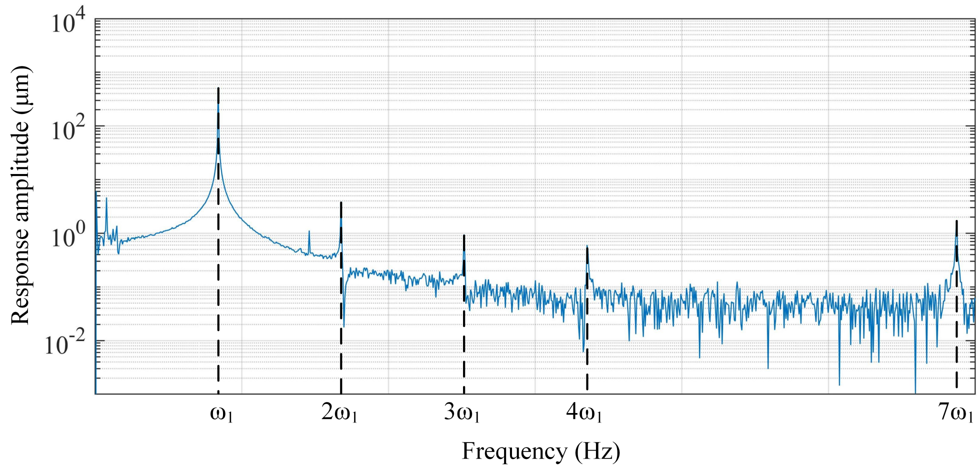


Figure 14: Response spectrum of response-amplitude-controlled fixed sine test at 10 g.

cameras [48]. Although several harmonics of the first mode are present, their amplitude is several orders of magnitude lower than the fundamental harmonic. In order to smooth the results, the data are filtered by a third-order bandpass butterworth filter centered at the first natural frequency with a bandwidth of 40% of the first natural frequency. The results of the mode shape estimation are shown in **Fig. 15** for each amplitude level, both for the upper and lower lines. Two additional plots shed further light on the amplitude-dependent properties of the mode shape. The first one, **Fig. 16** (a), shows the upper line mode shape of a central portion of the beam, normalized with respect to the left tip displacement. From the lowest to the highest excitation amplitude, the displacements of the central part of the

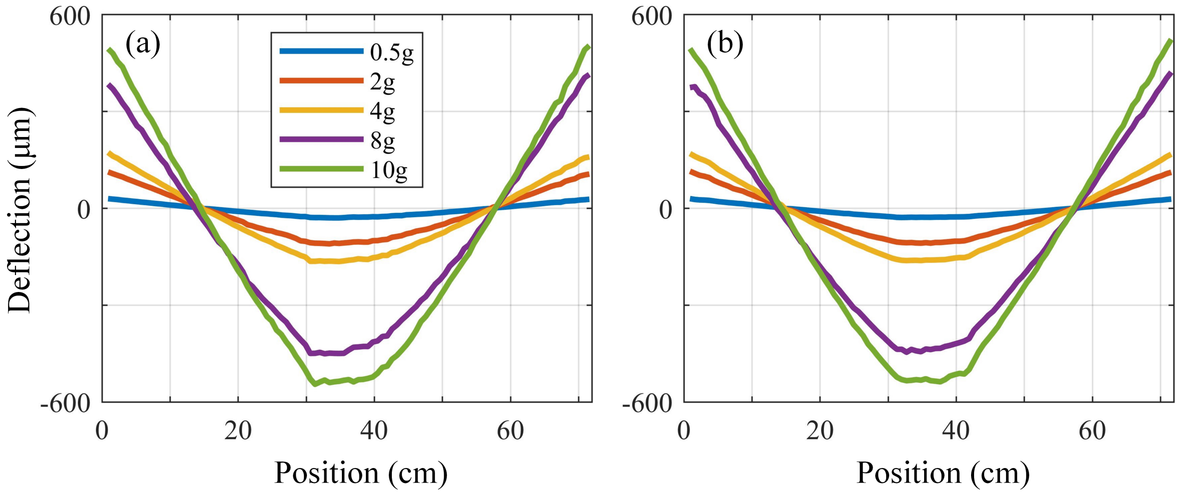


Figure 15: Amplitude-dependent mode shape of the $1^{st}$ mode of the HBRB from response-amplitude-controlled testing, showing (a) DIC lower line and (b) DIC upper line. Each line is the mode shape calculated from the maximum displacement for an excitation level.

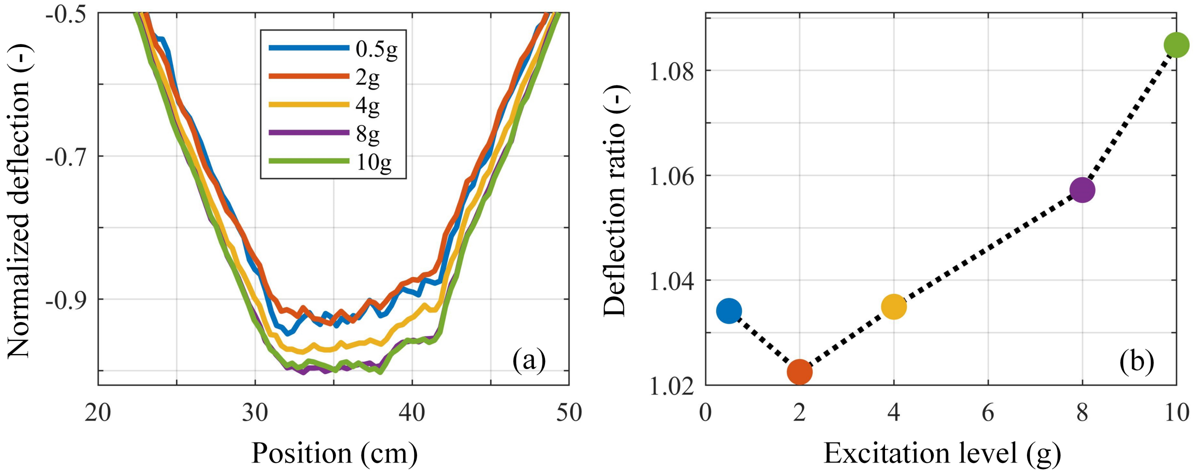


Figure 16: Amplitude-dependent mode shape of the $1^{st}$ mode of the HBRB from response-amplitude-controlled testing of DIC upper line, showing (a) normalized deflection and (b) deflection ratio between the middle of the beam to the tip displacement.

beam increase approximately by 7%, with respect to the tip displacement, but decrease for the 2 g level. This suggests a softening behavior of the modal stiffness. The overall trend resembles that of the backbone curve, but the variation in this case is greater with respect to the frequency change in the backbone curve, cf. **Fig. 8**, since this is a local phenomenon while the natural frequency depends on global characteristics. This behavior is illustrated more compactly in **Fig. 16** (b) with the deflection ratio between the displacement of the middle of the beam to the tip displacement. Precisely, the tip displacement is computed as the average between the displacements of the ten leftmost points from DIC, and the middle displacement is the average among the ten displacements around the beam center. While the locations of the mode shape nodes remain unchanged, the principal variation of the mode shape is concentrated in the middle of the beam, suggesting that further studies should connect this macroscopic observation with microscopic phenomena of the contact patch.

### *3.4.3. Energy of the Beam*

The total energy of a structure consists of kinetic energy and potential (strain) energy. As shown in the STFT analysis (**Fig. 5** (b)), the free decay response obtained from the shaker ringdown testing only contains the first mode of the HBRB. The potential energy is assumed to be zero at the equilibrium position, corresponding to the configuration when all displacements are zero. As verified previously, the vibration is synchronous and, during the decay, every point passes through zero at the same time. At these time instances, the total energy of the structure is therefore equal to the kinetic energy.

As DIC provides responses of a large number of points, the HBRB can be discretized into lumped mass elements. The filtered displacement responses (**Fig. 9** (b)) can be transferred into velocity responses by numerical differentiation. Thus, with the full-field information of the structure and the mass of the whole beam ($M = 1.796$ kg as measured), the energy $E$ at time instant $t$ can be approximated by

$$E(t) = \sum_{i=1}^{N} \frac{1}{2} m v_i^2(t), \tag{5}$$

where $N$ is the number of the measurement points, $v_i$ is the velocity of the $i$th point, and $m = M/N$ is the mass of each measurement point.

Here, the total number of the measurement points is $N = 206$, which is determined during the processing of the DIC. The energy trend, computed using all measurement points, over the shaker ringdown testing is shown in **Fig. 17** (a) with a black line, and the red dots depict energy peaks. In order to study the influence of the number of the measurement points on the calculation of $E$, $N$ is varied from 5 to 206 over an equally spaced grid. **Figure 17** (b) shows the energy of the beam, at the time instant of the first peak, as a function of $N$, which converges for $N > 100$. In other words, the number of points $N$ needed to have an accurate estimation of the energy is higher than 100. This spatial resolution is not achievable with contact sensors such as accelerometers or strain gauges, but only with a non-contact measurement approach, such as videography and DIC.

The relationships between energy and displacement/acceleration amplitudes for the accelerometer located on the shaker (see Accel 3 in **Fig. 2** (a)) is shown in **Fig. 17** (b). A clear, quadratic trend, as defined in Eq. (5), is observed. The accuracy of the energy calculation by DIC is validated in **Fig. 17** (d) by means of the dissipated energy. The red and green dots are the work done by the forcing for the response-control (red) and force-control (green) testing procedures for different amplitudes, cf. **Fig. 7** (b). These quantities are computed using the measurement of the shaker force and the acceleration of the driven point. As argued in **Sect. 3.2**, this work is equal to that done by the non-conservative forces over one oscillation cycle. For the shaker ringdown, the peaks in the kinetic energy correspond to the total energy of the system, since the motion is synchronous. Hence, the difference between the energy of the $k$-th peak and that of the $(k+2)$-th peak (see the inset in **Fig. 17** (a)) is the work done by the non-conservative forces in one oscillation cycle. The dissipative work computed from forced testing and from shaker ringdown is expected to be comparable from theoretical speculations. Indeed, **Fig. 17** (d) shows that there is a very good agreement with the two. Here, the blue line shows the dissipative work, computed using the kinetic energy decay obtained from full-field data, plotted against the acceleration amplitude level. It agrees well with the energy measurements obtained in forced testing using a single accelerometer.

The energy computed here could serve for model validation or tuning, but it is also useful to construct frequency-energy plots, typically adopted in the NNM literature [9] to characterize the dynamical feature of nonlinear responses. Frequency-energy plots are particularly meaningful for conservative systems, where each NNM orbit lies on a specific energy level [29]. However, they are relevant also for weakly forced, damped structures as their resonant periodic motions typically show small deviations from their conservative counterpart, which

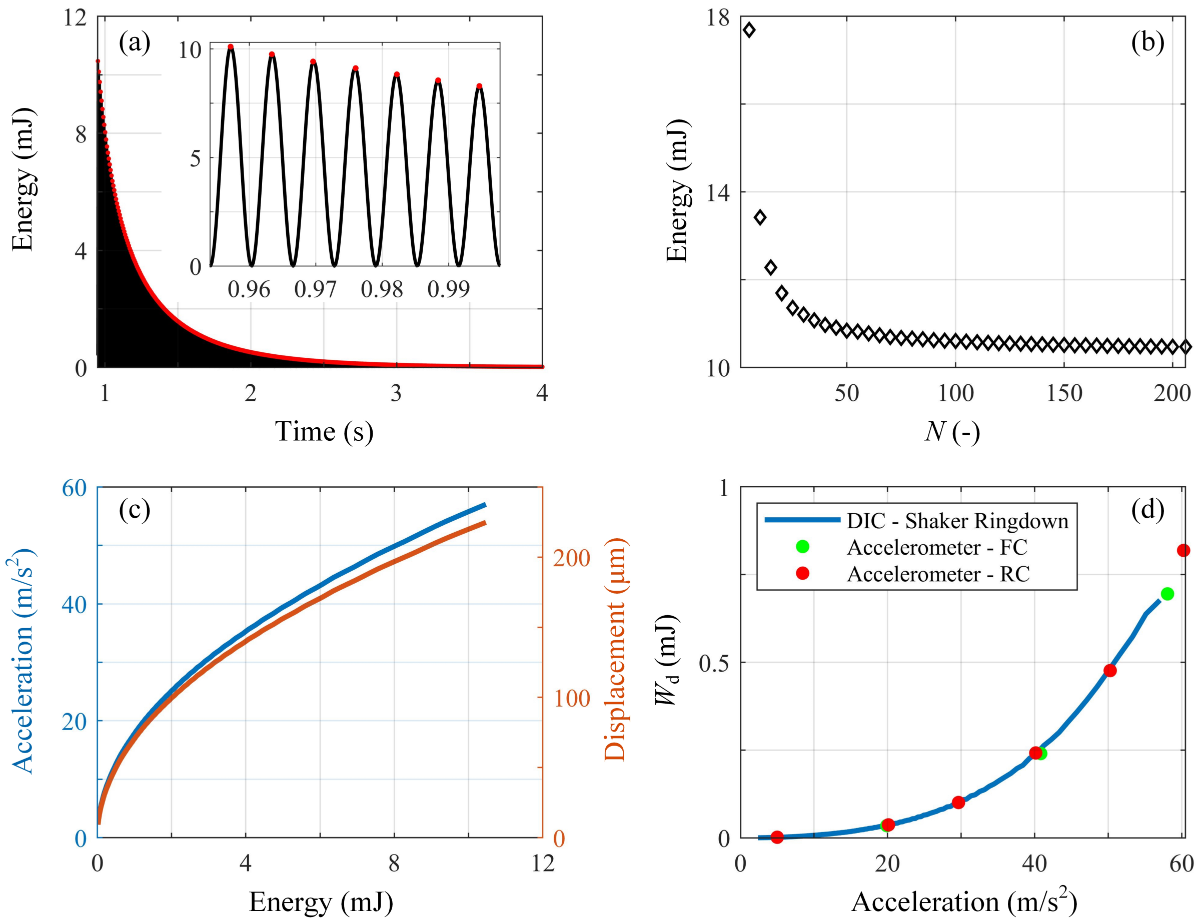


Figure 17: The energy of the HBRB where (a) shows the trend of the kinetic energy over time (with the inset showing the first seven peaks) and (b) the dependence of the energy on the number of the measurement points. Plot (c) shows the relation between energy and displacement/acceleration amplitudes at the location of Accel 3 in **Fig. 2**. The last plot in (d) shows the dissipated energy over one oscillation cycle computed via accelerometer measurements from forced testing (red and green dots, cf. **Sect. 3.2**) and the same quantity extracted using full-field data from shaker ringdown.

can be neglected [46, 47, 61]. Experimentally, the construction of frequency-energy plots is not practical since measuring the energy of a structure accurately is impractical with accelerometers, and thus the frequency-amplitude (typically acceleration amplitude) backbone plots are often reported instead, which is a flawed metric [19, 20]. In this study, however, the calculation of energy is feasible due to the full-field information from DIC.

**Figure 18** shows the nonlinear characteristics of the system using the full-field DIC data. Here, all of the 206 DIC points are considered to ensure a sufficiently converged result, since the use of $N = 206$ instead of a smaller value, such as 100, comes at no significant computational cost increase. As an alternative to the displacement or acceleration amplitude used previously (see **Figs. 8** or **11**), the damping and frequency are now combined with the energy calculations, as shown in **Fig. 18** (a)-(d). Specifically, **Fig. 18** (c) and (d)

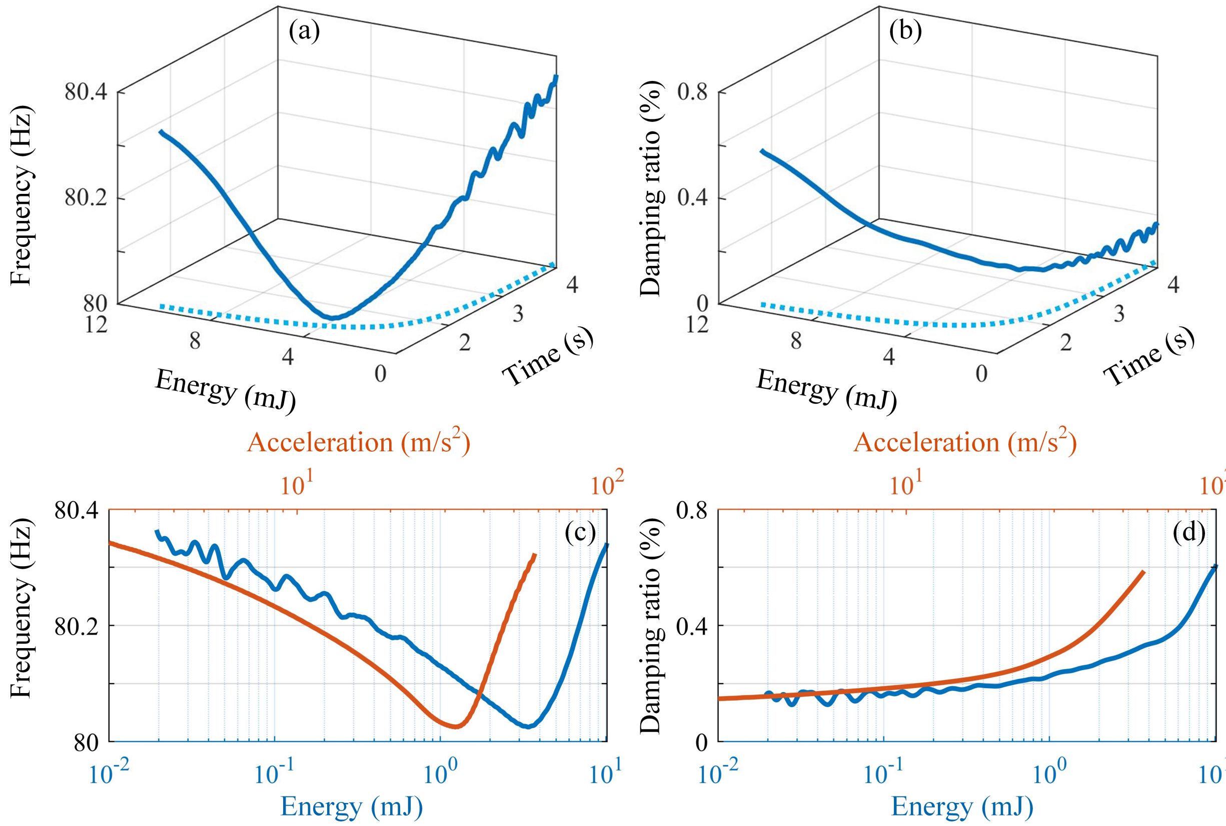


Figure 18: The relationship between the time, energy, amplitude, and nonlinear characteristics of the HBRB, including (a) relationship between time, energy, and frequency, (b) relationship between time, energy, and damping ratio, (c) energy-dependent and amplitude-dependent frequencies, (d) energy-dependent and amplitude-dependent damping ratios. The latter amplitudes refers to the acceleration amplitudes measured by Accel 3 in **Fig. 2**.

superimpose amplitude-dependence and energy-dependence. Clearly, the two properties show consistent values of frequency and damping whose amplitudes are related by a scaling factor and a quadratic relationship. Amplitude-dependent property plots act as proxies for the energy-dependent property plots in this case, but the latter may provide a more global perspective on the system under analysis. However, the energy-dependent plots in **Fig. 18** (c) and (d) show an increased variability towards small amplitudes, due to the degradation of the signal-to-noise ratio in DIC measurements. By contrast, amplitude-dependent curve shows a smoother behavior since the accelerometer data, at the same amplitudes, is not subject to these noise issues. It is important to note that if the system was not vibrating synchronously, the amplitude dependent plots may have a less clear relationship with the energy plots depending on which point is used to measure the amplitude.

## 4. Comparison of the Methods from a Practitioner Viewpoint

Nonlinear system identification, as shown in this paper, requires a toolbox approach in which different techniques have to be deployed depending on the system under analysis and the testing procedure. Force-response testing tends to provide robust information since steady states can be properly isolated, but the shaker unavoidably influences the system dynamics. Hammer excitation is easy to perform, but it generates a multi-modal component. This is less than ideal if the identification targets a particular mode of the structure, as much of the energy is distributed across modes that are not of interest. In this context, shaker ringdown should be the preferred test method as it combines the advantages from both shaker testing (i.e., single frequency and high level of excitation at that frequency) and hammer excitation (i.e., transient free decay data). However, decoupling the shaker from the structure is often not a straightforward task [48].

Excluding SS-SSM, all of the methods used in this paper are signal processing techniques suited for time-frequency analyses. The extraction of frequency patterns in a time series varies according to the theoretical foundations of the method, but a common requirement of time-frequency methods is the need to filter the transient data before extracting the nonlinear characteristics. By contrast, for SS-SSM, the frequency-amplitude relation is intrinsic in the identified nonlinear model of the system. Encouragingly, all of the techniques showed good agreement in the results for shaker ringdown and hammer testing.

Among all of the methods, DMD is the only one that was originally born for the analysis of multi-point measurements of the dynamical system. The other techniques are more suited for single-point measurements, and hence required suitable rearrangements in order to be applied to multiple measurements simultaneously. Moreover, the HT, PFF, SS-SSM, and WBEMD methods have been developed and extensively used for studying transient regimes in mechanical systems. By contrast, DMD, broadly known in the fluid dynamics community for unfolding the dynamics of ergodic attractors, has presented challenges for tackling transient phenomena [68]. However, the results of DMD show a very good agreement with the other techniques in the context of this research.

Every technique deployed in this paper presents either computational or implementation challenges. From the complexity viewpoint, all of the techniques have drawbacks. The HT and PFF methods require filtering that needs to be manually tuned for the best results [58] in order to retain the core harmonic information of the time series [25]. Moreover, the HT method suffers from the issue of end effect in the estimation of the damping curve, even though appropriate signal pre-processing is performed, cf. **Fig. 4** (b) and see [25]. For the SS-SSM method, model fitting is fundamental for obtaining adequate results [34], which requires a computational routine to determine the coefficients that describe the SSM and its dynamics [31]. For DMD, the results depend on the selection of time scales (e.g., sampling, windowing) and of the number of dynamic modes. Finally, WBEMD needs an optimization in order to identify the intrinsic mode functions, and hence it requires some application dependent parameters [57]. Overall, DMD, HT, and PFF may seem to be less complex in terms of implementation for the context of the paper. However, SS-SSM may also be exploited to construct data-driven reduced models, and WBEMD can efficiently uncover multi-modal transient phenomena.

## 5. Conclusions

This paper compared the performance of multiple nonlinear identification methods based on the experimental data from a jointed structure. The backbone curve and amplitude-damping curve were extracted from the signals using Hilbert Transform (HT), Peak Finding and Fitting (PFF), Dynamic Mode Decomposition (DMD), State-Space Spectral Submanifold (SS-SSM), and Wavelet-Bounded Empirical Mode Decomposition (WBEMD). The responses were measured by accelerometers in the experiments including hammer testing, shaker ringdown testing, and response/force-control stepped sine testing. During the shaker ringdown testing, apart from the accelerometers, two high-speed cameras recorded the images of the jointed beam. Then, Digital Image Correlation (DIC) was adopted to extract the displacement responses from the images to reconstruct the mode shapes of the whole beam. The main conclusions of this paper are summarized as follows:

- Backbone and damping curves obtained from hammer testing and shaker ringdown testing showed a similar trend. However, the amplitude range in the shaker ringdown testing was wider than that in the hammer testing despite the peak amplitude of the acceleration of the tip of the beam being smaller in the shaker tests. This happens because the hammer testing excites multiple modes, while the shaker ringdown testing is able to excite one single mode of the structure. Especially at high amplitudes, the amplitude-dependent properties obtained via hammer testing deviated from those obtained via shaker ringdown testing, although proper filtering was applied. This observation proves that other modes can indeed influence the amplitude-dependent properties of a specific mode. Therefore, hammer testing should be carefully handled when aiming to extract single-mode nonlinear information.

- Amplitude-dependent properties computed from shaker ringdown testing and from forced-response testing presented good agreement, as expected from theoretical results. In this paper, an energy criterion was used to extract backbone and damping curves from response/forced-control testing. Although it requires precise tuning and an effective decoupling mechanism, shaker ringdown testing is more efficient with respect to forced testing, where the acquisition of dense datasets can necessitate extensive experimental campaigns.

- Other than amplitude-dependent properties, which show good agreement with those coming from accelerometer data, full-field data from two high-speed cameras are able to reconstruct the mode shape of the beam. The deformation induced by the lap joint is visible and the variation of the mode shape with the amplitude of motion can be assessed as well as motion synchronism. Moreover, full-field data allows the definition of the kinetic energy of the beam, which is able to determine amplitude-dependent properties. The value of the kinetic energy also showed good convergence properties as the number of measurement points was increased. Moreover, the dissipated energy computed from the decay of kinetic energy during a shaker ringdown test is consistent with the dissipated energy computed in forced testing. The metric of energy, which cannot be achieved with traditional accelerometers alone due to the need for a spatially dense data set for adequate convergence, can be useful for practices such as model validation and model updating. However, especially when dealing with long structures in free vibrations, the cameras are limited in memory, and thus they are only able to record a short period of time.

- All of the methods used in the paper agreed well in the extraction of amplitude-dependent properties from free vibrations. Other than showing performances, this paper also critically compared these methods, pointing out benefits and potential challenges in order to enrich the toolbox of practitioners in structural dynamics.

- In terms of the frequency-amplitude and damping-amplitude curves, the beam under investigation showed limited frequency change, i.e., 0.5 Hz, while the damping ratio rose from about 0.1% at low amplitude to more than 0.6% at high amplitudes. Additionally, the mode shape presented substantial amplitude dependence, especially in the area of the contact patch. The deflection ratio, which tries to quantify this variation, exhibited a similar trend to that of the backbone curve, but with a much wider range amounting to 7%. Thus, the strongest nonlinearities for the jointed beam studied were observed in the damping behavior and the variation of the mode shape. Further studies can help to uncover the connection of these macroscopic phenomena with interactions occurring in the contact patch.

- The relationship between the energy and nonlinear frequency and damping ratio of the beam have been obtained due to the full-field DIC data. The energy-dependent characteristics provide the information of the whole beam instead of a few points on the structure. Accelerometers, as a traditional way of measurement, make the measurement of the beam's energy prohibitively difficult since it is not practical to place a large number (i.e., 100s) of accelerometers on this specific structure, let alone the effect of the added mass. By contrast, high-speed cameras provide a convenient way of measuring the structure without contact. Additionally, responses of the structure can be obtained with a high spatial resolution, making it possible to accomplish the identification of the whole structure.

## Acknowledgments

. This paper shows the work done in the 2019 Tribomechadynamics Research Camp. The authors appreciate this chance to work together. The authors would like to thank SIEMENS and South Central Imaging for their sponsorship. The authors from Tongji University want to thank the China Scholarship Council (CSC) for financial support at Rice University.

The author GK has been supported by the European Union's Horizon 2020 research and innovation program under the Marie Skłodowska-Curie grant agreement No 764547. The author DJ has been generously supported by the SERB fellowship.

## Data Access

The data used in the paper is available at `https://github.com/mattiacenedese/BRBtesting`.

## References


[1] M. R. W. Brake (Ed.). *The mechanics of jointed structures: recent research and open challenges for developing predictive models for structural dynamics.* Springer, Cham, Switzerland, 2017.

[2] L. Gaul and J. Lenz. Nonlinear dynamics of structures assembled by bolted joints. *Acta Mechanica*, 125(1-4):169–181, 1997.

[3] M. M. Alamdari, J. Li, B. Samali, H. Ahmadian, and A. Naghavi. Nonlinear joint model updating in assembled structures. *Journal of Engineering Mechanics*, 140(7), 2014.

[4] A. Fantetti, L. R. Tamatam, M. Volvert, I. Lawal, L. Liu, L. Salles, M. R. W. Brake, C. W. Schwingshackl, and D. Nowell. The impact of fretting wear on structural dynamics: Experiment and simulation. *Tribology International*, 138:111–124, 2019.

[5] W. Chen, M. Jin, I. Lawal, M. R. W. Brake, and H. Song. Measurement of slip and separation in jointed structures with non-flat interfaces. *Mechanical Systems and Signal Processing*, 134:106325, 2019.

[6] J. P. Noël, L. Renson, and G. Kerschen. Complex dynamics of a nonlinear aerospace structure: Experimental identification and modal interactions. *Journal of Sound and Vibration*, 333(12):2588–2607, 2014.

[7] K. Worden, D. Hickey, M. Haroon, and D. E. Adams. Nonlinear system identification of automotive dampers: A time and frequency-domain analysis. *Mechanical Systems and Signal Processing*, 23(1):104–126, 2009.

[8] T. W. Jerome, M. R. Shepherd, and S. A. Hambric. *Acoustic Excitation of a Flanged Joint*, pages 211–224. Conference Proceedings of the Society for Experimental Mechanics Series. Springer International Publishing Ag, Cham, 2019.

[9] G. Kerschen, K. Worden, A. F. Vakakis, and J. C. Golinval. Past, present and future of nonlinear system identification in structural dynamics. *Mechanical Systems and Signal Processing*, 20(3):505–592, 2006.

[10] J. M. Londoño, S. A. Neild, and J. E. Cooper. Identification of backbone curves of nonlinear systems from resonance decay responses. *Journal of Sound and Vibration*, 348:224–238, 2015.

[11] T. Breunung and G. Haller. Explicit backbone curves from spectral submanifolds of forced-damped nonlinear mechanical systems. *Proceedings of the Royal Society A*, 474(2213):20180083, 2018.

[12] J. M. Londoño, S. A. Neild, and J. E. Cooper. Systems with bilinear stiffness: Extraction of backbone curves and identification. *IMAC XXXIII A Conference and Exposition on Structural Dynamics*, Orlando, FL, February, 2015.

[13] D. J. Ewins, B. Weekes, and A. delli Carri. Modal testing for model validation of structures with discrete nonlinearities. *Philosophical Transactions of the Royal Society A: Mathematical, Physical and Engineering Sciences*, 373(2051):20140410, 2015.

[14] D. J. Ewins. Exciting vibrations: the role of testing in an era of supercomputers and uncertainties. *Meccanica*, 51:3241–3258, 2016.

[15] S. A. Smith, M. R. W. Brake, and C. W. Schwingshackl. On the characterization of nonlinearities in assembled structures. *Journal of Vibration and Acoustics*, 142(5):11, 2020.

[16] D. Roettgen, M. S. Allen, D. Kammer, and R. L. Mayes. Substructuring of a nonlinear beam using a modal Iwan framework, Part I: Nonlinear modal model identification. *IMAC XXXV A Conference and Exposition on Structural Dynamics*, Garden Grove, CA, January, 2017.

[17] A. Akay. Research needs and open questions in vibration energy transport and dissipation. Technical Report Forthcoming, National Science Foundation, 2016.

[18] M. R. W. Brake, C. W. Schwingshackl, and P. Reuss. Observations of variability and repeatability in jointed structures. *Mechanical Systems and Signal Processing*, 129:282–307, 2019.

[19] S. Schwarz, L. Kohlmann, A. Hartung, J. Gross, M. Scheel, and M. Krack. Validation of a turbine blade component test with frictional contacts by phase-locked-loop and force-controlled measurements. *Journal of Engineering for Gas Turbines Power*, 142(5):051006, 2020.

[20] T. Heinze, L. Panning-von Scheidt, and J. Wallaschek. Global detection of detached periodic solution branches of friction-damped mechanical systems. *Nonlinear Dynamics*, 99:1841–1870, 2020.

[21] M. Krack. Extension of the single-nonlinear-mode theory by linear attachments and application to exciter-structure interaction. *Under Review*, 2020.

[22] M. Feldman. Non-linear system vibration analysis using Hilbert transform—I. Free vibration analysis method 'Freevib'. *Mechanical Systems and Signal Processing*, 8(2):119–127, 1994.

[23] M. Feldman. Hilbert transform in vibration analysis. *Mechanical Systems and Signal Processing*, 25(3):735–802, 2011.

[24] M. Jin, M. R. W. Brake, and H. Song. Comparison of nonlinear system identification methods for free decay measurements with application to jointed structures. *Journal of Sound and Vibration*, 453:268–293, 2019.

[25] M. Jin, W. Chen, M. R. W. Brake, and H. Song. Identification of instantaneous frequency and damping from transient decay data. *Journal of Vibration and Acoustics*, 142(5):051111, 2020.

[26] P. J. Schmid. Dynamic mode decomposition of numerical and experimental data. *Journal of Fluid Mechanics*, 656:5–28, 2010.

[27] H. Arbabi and I. Mezic. Ergodic theory, dynamic mode decomposition, and computation of spectral properties of the Koopman operator. *SIAM Journal on Applied Dynamical Systems*, 16(4):2096–2126, 2017.

[28] J. H. Tu, C. W. Rowley, D. M. Luchtenburg, S. L. Brunton, and J. N. Kutz. On dynamic mode decomposition: Theory and applications. *Physics*, 1(2):391–421, 2014.

[29] G. Kerschen, M. Peeters, J. C. Golinval, and A. F. Vakakis. Nonlinear normal modes, Part I: A useful framework for the structural dynamicist. *Mechanical Systems and Signal Processing*, 23(1):170–194, 2009.

[30] G. Haller and S. Ponsioen. Nonlinear normal modes and spectral submanifolds: existence, uniqueness and use in model reduction. *Nonlinear Dynamics*, 86(3):1493–1534, 2016.

[31] S. Ponsioen, T. Pedergnana, and G. Haller. Automated computation of autonomous spectral submanifolds for nonlinear modal analysis. *Journal of Sound and Vibration*, 420:269 – 295, 2018.

[32] S. Ponsioen, T. Pedergnana, and G. Haller. Analytic prediction of isolated forced response curves from spectral submanifolds. *Nonlinear Dynamics*, 98(4):2755–2773, 2019.

[33] G. Haller and S. Ponsioen. Exact model reduction by a slow–fast decomposition of nonlinear mechanical systems. *Nonlinear Dynamics*, 90(1):617–647, 2017.

[34] R. Szalai, D. Ehrhardt, and G. Haller. Nonlinear model identification and spectral submanifolds for multi-degree-of-freedom mechanical vibrations. *Proceedings of the Royal Society A-Mathematical Physical and Engineering Sciences*, 473(2202), 2017.

[35] N. E. Huang, Z. Shen, S. R. Long, M. L. C. Wu, H. H. Shih, Q. N. Zheng, N. C. Yen, C. C. Tung, and H. H. Liu. The empirical mode decomposition and the Hilbert spectrum for nonlinear and non-stationary time series analysis. *Proceedings of the Royal Society A-Mathematical Physical and Engineering Sciences*, 454(1971):903–995, 1998.

[36] K. J. Moore, M. Kurt, M. Eriten, D. M. McFarland, L. A. Bergman, and A. F. Vakakis. Wavelet-bounded empirical mode decomposition for vibro-impact analysis. *Nonlinear Dynamics*, 93(3):1559–1577, 2018.

[37] N. N. Balaji and M. R. W. Brake. The surrogate system hypothesis for joint mechanics. *Mechanical Systems and Signal Processing*, 126:42–64, 2019.

[38] J. P. Noël and G. Kerschen. Nonlinear system identification in structural dynamics: 10 more years of progress. *Mechanical Systems and Signal Processing*, 83:2–35, 2017.

[39] M. Peeters, R. Viguie, G. Serandour, G. Kerschen, and J. C. Golinval. Nonlinear normal modes, Part II: Toward a practical computation using numerical continuation techniques. *Mechanical Systems and Signal Processing*, 23(1):195–216, 2009.

[40] P. Reu. Introduction to digital image correlation: Best practices and applications. *Experimental Techniques*, 36(1):3–4, 2012.

[41] P. L. Reu, D. P. Rohe, and L. D. Jacobs. Comparison of DIC and LDV for practical vibration and modal measurements. *Mechanical Systems and Signal Processing*, 86:2–16, 2017.

[42] Brøns M., Kasper T. A., Chauda G., Klaassen S. W. B., C. W. Schwingshackl, and Brake M. R. W. Experimental investigation of local dynamics in a bolted lap joint using digital image correlation. *Journal of Vibration and Acoustics*, 142(5), 2020.

[43] D. A. Ehrhardt and M. S. Allen. Measurement of nonlinear normal modes using multi-harmonic stepped force appropriation and free decay. *Mechanical Systems and Signal Processing*, 76-77:612 – 633, 2016.

[44] S. Peter, M. Scheel, M. Krack, and R. I. Leine. Synthesis of nonlinear frequency responses with experimentally extracted nonlinear modes. *Mechanical Systems and Signal Processing*, 101:498 – 515, 2018.

[45] L. Renson, A. Gonzalez-Buelga, D.A.W. Barton, and S.A. Neild. Robust identification of backbone curves using control-based continuation. *Journal of Sound and Vibration*, 367:145 – 158, 2016.

[46] M. Peeters, G. Kerschen, and J. C. Golinval. Dynamic testing of nonlinear vibrating structures using nonlinear normal modes. *Journal of Sound and Vibration*, 330(3):486–509, 2011.

[47] M. Peeters, G. Kerschen, and J. C. Golinval. Modal testing of nonlinear vibrating structures based on nonlinear normal modes: Experimental demonstration. *Mechanical Systems and Signal Processing*, 25(4):1227–1247, 2011.

[48] W. Chen, D. Jana, A. Singh, M. Jin, M. Cenedese, G. Kosova, M. W. R. Brake, C. W. Schwingshackl, S. Nagarajaiah, K. Moore, and J. P. Noël. Measurement and identification of the nonlinear dynamics of a jointed structure using full-field data; Part I - Measurement of nonlinear dynamics. *Preprint*, 2021.

[49] D. R. Roettgen and M. S. Allen. Nonlinear characterization of a bolted, industrial structure using a modal framework. *Mechanical Systems and Signal Processing*, 84:152–170, 2017.

[50] M. Feldman. Hilbert transform methods for nonparametric identification of nonlinear time varying vibration systems. *Mechanical Systems and Signal Processing*, 47(1-2):66–77, 2014.

[51] T. Dossogne, T.W. Jerome, D.P.T. Lancereau, S.A. Smith, M.R.W. Brake, B.R. Pacini, P. Reuss, and C.W. Schwingshackl. Experimental assessment of jointed configuration. *IMAC XXXV A Conference and Exposition on Structural Dynamics*, Garden Grove, CA, January, 2017.

[52] P. F. Pai and A. N. Palazotto. HHT-based nonlinear signal processing method for parametric and non-parametric identification of dynamical systems. *International Journal of Mechanical Sciences*, 50(12):1619–1635, 2008.

[53] M. Cenedese and G. Haller. Constructing backbone curves from free-decay vibrations data in multi-degrees of freedom oscillatory systems. In G. Kerschen, M. R. W. Brake, and L. Renson, editors, *Nonlinear Structures and Systems, Volume 1*, page 221–223. Springer International Publishing, Cham, 2020.

[54] J. N. Juang and R. S. Pappa. An eigensystem realization-algorithm for modal parameter-identification and model-reduction. *Journal of Guidance Control and Dynamics*, 8(5):620–627, 1985.

[55] K. J. Moore, A. Mojahed, M. Kurt, M. Eriten, D. M. McFarland, L. A. Bergman, and A. F. Vakakis. *Advanced Nonlinear System Identification for Modal Interactions in Nonlinear Structures: A Review*, pages 101–118. Springer International Publishing, Cham, Switzerland, 2019.

[56] N. E. Huang, M. C. Wu, S. R. Long, S. S. P. Shen, W. Qu, P. Gloersen, and K. L. Fan. A confidence limit for the empirical mode decomposition and Hilbert spectral analysis. *Proceedings of the Royal Society A*, 459(2037):2317–2345, 2003.

[57] K. J. Moore, M. Kurt, M. Eriten, D. M. McFarland, L. A. Bergman, and A. F. Vakakis. Wavelet-bounded empirical mode decomposition for measured time series analysis. *Mechanical Systems and Signal Processing*, 99:14–29, 2018.

[58] H. G. D. Goyder and D. P. T. Lancereau. Extracting natural frequencies and damping from time histories. better than the frequency domain? *ISMA International Conference on Noise and Vibration Engineering*, KU Leuven, 2018.

[59] C. W. Schwingshackl, C. Joannin, L. Pesaresi, J. S. Green, and N. Hoffmann. Test method development for nonlinear damping extraction of dovetail joints. *IMAC XXXII A Conference and Exposition on Structural Dynamics*, Orlando, FL, February, 2014.

[60] J. P. Noël, L. Renson, C. Grappasonni, and G. Kerschen. Identification of nonlinear normal modes of engineering structures under broadband forcing. *Mechanical Systems and Signal Processing*, 74:95–110, 2016.

[61] M. Cenedese and G. Haller. How do conservative backbone curves perturb into forced responses? A Melnikov function analysis. *Proceedings of the Royal Society of London A: Mathematical, Physical and Engineering Sciences*, 476:20190494, 2020.

[62] M. Cenedese and G. Haller. Stability of forced–damped response in mechanical systems from a Melnikov analysis. *Chaos: An Interdisciplinary Journal of Nonlinear Science*, 30(8):083103, 2020.

[63] M. Krack. Nonlinear modal analysis of nonconservative systems: Extension of the periodic motion concept. *Computers & Structures*, 154:59 – 71, 2015.

[64] Y. Sun, A. Vizzaccaro, J. Yuan, and L. Salles. An extended energy balance method for resonance prediction in forced response of systems with non-conservative nonlinearities using damped nonlinear normal mode. *Nonlinear Dynamics*, 103(4):3315–3333, 2021.

[65] W. Chen, M. Jin, I. Lawal, M. R. W. Brake, and H. Song. Measurement of slip and separation in jointed structures with non-flat interfaces. *Mechanical Systems and Signal Processing*, 134:106325, 2019.

[66] M. Brøns, T. A. Kasper, G. Chauda, S. W. B. Klaassen, C. W. Schwingshackl, and M. R. W. Brake. Experimental investigation of local dynamics in a bolted lap joint using digital image correlation. *Journal of Vibration and Acoustics*, 142(5):051114, 2020.

[67] R. M. Rosenberg. The normal modes of nonlinear n-degree-of-freedom systems. *Journal of Applied Mechanics*, 29:7–14, 1962.

[68] S. L. Brunton and J. N. Kutz. *Data-Driven Science and Engineering: Machine Learning, Dynamical Systems, and Control.* Cambridge University Press, Cambridge, UK, 2019.